

A joint study of early and late spectral distortions of the cosmic microwave background and of the millimetric foreground

R. Salvaterra¹ & C. Burigana²

¹SISSA/ISAS, Astrophysics Sector, Via Beirut, 4, I-34014 Trieste, Italy

²IASF/CNR, Istituto di Astrofisica Spaziale e Fisica Cosmica, Sezione di Bologna, Consiglio Nazionale delle Ricerche, Via Gobetti 101, I-40129 Bologna, Italy

Submitted to MNRAS, 14 March 2002; in this revised version, 17 June 2002; accepted, 19 June 2002.

ABSTRACT

In this work we have compared the absolute temperature data of the CMB spectrum with models of CMB spectra distorted by a single or two heating processes at different cosmic times. The constraints on the fractional energy injected in the radiation field, $\Delta\epsilon/\epsilon_i$, are mainly provided by the precise measures of the FIRAS instrument aboard the COBE satellite, while long wavelength measures are crucial to set constraints on free-free distortions. We find that the baryon density does not influence the limits on $\Delta\epsilon/\epsilon_i$ derived from current data for cosmic epochs corresponding to the same dimensionless time y_h of dissipation epoch, although the redshift corresponding to the same y_h decreases with the baryon density. Under the hypothesis that two heating processes have occurred at different epochs, the former at any y_h in the range $5 \geq y_h \geq 0.01$ (this joint analysis is meaningful for $y_h \gtrsim 0.1$) and the latter at $y_h \ll 1$, the limits on $\Delta\epsilon/\epsilon_i$ are relaxed by a factor ~ 2 both for the earlier and the later process with respect to the case in which a single energy injection in the thermal history of the universe is considered. In general, the constraints on $\Delta\epsilon/\epsilon_i$ are weaker for early processes ($5 \gtrsim y_h \gtrsim 1$) than for relatively late processes ($y_h \lesssim 0.1$), because of the sub-centimetric wavelength coverage of FIRAS data, relatively more sensitive to Comptonization than to Bose-Einstein like distortions.

While from a widely conservative point of view the FIRAS calibration as revised by Battistelli et al. 2000 only implies a significant relaxation of the constraints on the Planckian shape of the CMB spectrum, the favourite calibrator emissivity law proposed by the authors, quite different from a constant emissivity, implies significant deviations from a Planckian spectrum. An astrophysical explanation of this, although intriguing, seems difficult. We find that an interpretation in terms of CMB spectral distortions should require a proper balance between the energy exchanges at two very different cosmic times or a delicate fine tuning of the parameters characterizing a dissipation process at intermediate epochs, while an interpretation in terms of a relevant millimetric foreground, produced by cold dust, should imply a too large involved mass and/or an increase of the fluctuations at sub-degree angular scales. Future precise measurements at longer wavelengths as well as current and future CMB anisotropy space missions will provide independent, direct or indirect, cross checks.

This work is related to PLANCK-LFI activities.

Key words: cosmology: cosmic microwave background – spectral distortions – foregrounds

1 INTRODUCTION

As widely discussed in many papers, the spectrum of the cosmic microwave background (CMB) carries unique informations on physical processes occurring at early cosmic epochs (see, e.g., Danese & Burigana 1993 and references therein). The comparison between theoretical models of CMB spectral distortions and CMB absolute temperature measures can constrain the physical parameters of the considered dissipation processes. We improve here the previous analyses of the implications of the CMB spectrum data by jointly considering distortions generated in a wide range of early or intermediate cosmic epochs and at late cosmic epochs. We consider also the implications of a recent analysis of the COBE/FIRAS calibration by Battistelli et al. 2000, which suggests a decrement of the absolute temperature with the wavelength.

In section 2 we briefly summarize the general properties of the CMB spectral distortions, the main physical informations that can be derived from the comparison with the observations, and the relationship between the detection of possible CMB spectral distortions and the evaluation of the level of astrophysical sub-millimetric and millimetric foregrounds. The data sets used in this study are presented in section 3. In section 4 we present the constraints on CMB spectral distortions based on ground and balloon experiments and on the “standard” COBE/FIRAS data calibrated according to the COBE/FIRAS team (Mather et al. 1999 and references therein) for the case of a single and of a double energy injection in the thermal history of the universe. The extrapolation at very high redshifts and the impact of free-free distortions are considered in sections 5 and 6. In section 7 we analyse the implications of the calibration by Battistelli et al. 2000, by briefly reporting the main properties of their revised monopole spectral shape, and by jointly evaluating its impact on the CMB spectral distortion constraints and for the millimetric foreground. Finally, we draw our main conclusions in section 8.

2 THEORETICAL FRAMEWORK AND DATA EXPLOITATION

The CMB spectrum emerges from the thermalization redshift, $z_{therm} \sim 10^6 \div 10^7$, with a shape very close to a Planckian one, owing to the strict coupling between radiation and matter through Compton scattering and photon production/absorption processes, radiative Compton and Bremsstrahlung, which were extremely efficient at early times and able to re-establish a blackbody (BB) spectrum from a perturbed one on timescales much shorter than the expansion time (see, e.g., Danese & De Zotti 1977). The value of z_{therm} (Burigana et al. 1991a) depends on the baryon density (in units of the critical density), Ω_b , and the Hubble constant, H_0 , through the product $\widehat{\Omega}_b = \Omega_b (H_0/50)^2$ (H_0 expressed in Km/s/Mpc).

On the other hand, physical processes occurring at redshifts $z < z_{therm}$ may lead imprints on the CMB spectrum.

2.1 General properties of the CMB spectral distortions

The timescale for the achievement of kinetic equilibrium between radiation and matter (i.e. the relaxation time for the photon spectrum), t_C , is

$$t_C = t_{\gamma e} \frac{mc^2}{kT_e} \simeq 4.5 \times 10^{28} (T_0/2.7 K)^{-1} \phi^{-1} \widehat{\Omega}_b^{-1} (1+z)^{-4} \text{ sec}, \quad (1)$$

where $t_{\gamma e} = 1/(n_e \sigma T_C)$ is the photon-electron collision time, $\phi = (T_e/T_r)$, T_e being the electron temperature and $T_r = T_0(1+z)$; kT_e/mc^2 is the mean fractional change of photon energy in a scattering of cool photons off hot electrons, i.e. $T_e \gg T_r$; T_0 is the present radiation temperature related to the present radiation energy density by $\epsilon_{r0} = aT_0^4$; a primordial helium abundance of 25% by mass is here assumed.

It is useful to introduce the dimensionless time variable $y_e(z)$ defined by

$$y_e(z) = \int_t^{t_0} \frac{dt}{t_C} = \int_1^{1+z} \frac{d(1+z)}{1+z} \frac{t_{exp}}{t_C}, \quad (2)$$

where t_0 is the present time and t_{exp} is the expansion time given by

$$t_{exp} \simeq 6.3 \times 10^{19} \left(\frac{T_0}{2.7 K} \right)^{-2} (1+z)^{-3/2} \left[\kappa(1+z) + (1+z_{eq}) - \left(\frac{\Omega_{nr} - 1}{\Omega_{nr}} \right) \left(\frac{1+z_{eq}}{1+z} \right) \right]^{-1/2} \text{ sec}, \quad (3)$$

$z_{eq} = 1.0 \times 10^4 (T_0/2.7 K)^{-4} \widehat{\Omega}_{nr}$ being the redshift of equal non relativistic matter and photon energy densities (Ω_{nr} is the density of non relativistic matter in units of critical density); $\kappa = 1 + N_\nu (7/8)(4/11)^{4/3}$, N_ν being the number of relativistic, 2-component, neutrino species (for 3 species of massless neutrinos, $\kappa \simeq 1.68$), takes into account the contribution of relativistic neutrinos to the dynamics of the universe^{*}.

* Strictly speaking the present ratio of neutrino to photon energy densities, and hence the value of κ , is itself a function of the amount of energy dissipated. The effect, however, is never very important and is negligible for very small distortions.

Burigana et al. 1991b have reported on numerical solutions of the Kompaneets equation (Kompaneets 1956) for a wide range of values of the relevant parameters.

The analysis of the constraints on the thermal history of the universe set by the high accuracy measurements that have been recently accumulated requires the use of manageable formulae describing spectral distortions for a wide range of the relevant parameters.

Under the assumptions of *i*) small distortions, *ii*) dissipative processes with negligible photon production, *iii*) heating close to be instantaneous, a good approximation if the timescale for energy dissipation is much smaller than the expansion timescale, *iv*) distorted radiation spectrum initially represented by a superposition of blackbodies, as is the case for a broad variety of situations of cosmological interest, Burigana et al. 1995 found accurate analytical representations of the numerical solutions for the photon occupation number η computed by Burigana et al. 1991b. The CMB distorted spectra depend on at least three main parameters: the fractional amount of energy exchanged between matter and radiation, $\Delta\epsilon/\epsilon_i$, ϵ_i being the radiation energy density before the energy injection, the redshift z_h at which the heating occurs, and the baryon density $\hat{\Omega}_b$. The photon occupation number can be then expressed in the form

$$\eta = \eta(x; \Delta\epsilon/\epsilon_i, y_h, \hat{\Omega}_b), \quad (4)$$

where x is the dimensionless frequency $x = h\nu/kT_0$ (ν being the present frequency), and $y_h \equiv y_e(z_h)$ characterizes the epoch when the energy dissipation occurred, z_h being the corresponding redshift (we will refer to $y_h \equiv y_e(z_h)$ computed assuming $\phi = 1$, so that the epoch considered for the energy dissipation does not depend on the amount of released energy).

The form of these analytical approximations is in part suggested by the general properties of the Kompaneets equation and by its well known asymptotic solutions. For late distortions ($y_h \ll 1$) a superposition of blackbodies is, to a very good approximation, a solution of the Kompaneets equation, except at very low frequencies where photon emission processes are important; when they dominate the Kompaneets equation reduces to an ordinary differential equation. The Comptonization distortion produced by hot gas at small z is a typical example of superposition of blackbodies (Zeldovich & Sunyaev 1969; Zeldovich et al. 1972). At the other extreme (early distortions, $y_h \gtrsim 5$) the solution is well described by a Bose-Einstein (BE) formula with a frequency dependent chemical potential. For intermediate values of y_h , η has a shape somewhere between these two limiting cases. The shape of the distorted spectra at long wavelengths is characterized by a spread minimum of the brightness temperature for $y_h \lesssim 0.5$, and by a minimum at a well defined wavelength for $y_h \gtrsim 0.5$. The continuous behaviour of the distorted spectral shape with y_h can be in principle used also to search for constraints on the epoch of the energy exchange.

Of course, by combining the approximations describing the distorted spectrum at early and intermediate epochs with the Comptonization distortion expression describing late distortions, we are able to jointly treat two heating processes.

We remember that the adopted analytical description of the distorted spectrum holds also for continuous heating processes, i.e. by relaxing the above assumption *iii*), provided that they occur at quite late epochs ($y_h \lesssim 0.05$) or at early epochs ($y_h \gtrsim 5$), because of the properties of the asymptotic solutions. In the former case, $\Delta\epsilon/\epsilon_i$ is the dissipation rate integrated over the relevant time interval; in the latter case, the proper value of $\Delta\epsilon/\epsilon_i$ to be used in eq. (4) is given by $\simeq \mu(y_h \simeq 5)/1.4$, where $\mu(y_h \simeq 5)$ is the chemical potential at $y_h \simeq 5$ produced by the combined effect of the dissipation rate integrated over the time (which increases μ) and of radiative Compton and Bremsstrahlung (which decrease μ). In this case, eq. (4) represents a good approximation of the distorted spectrum by relaxing also the above assumption *ii*) provided that the combined effect of energy injection and photon production is properly included in the computation of the chemical potential $\simeq \mu(y_h \simeq 5)$ (see, e.g., Danese & Burigana 1993). For continuous processes at intermediate epochs ($5 \gtrsim y_h \gtrsim 0.05$), the above representation, with a proper “effective” value of y_h , can be used as a first order approximation of the distorted spectrum. Finally, for dissipation processes widely distributed in time, from $y_h \gtrsim 5$ to $y_h \ll 1$ (as some of those discussed in section 7.6, such as the damping of perturbations and the vacuum decay), the detailed final spectrum shape will depend on the details of the considered process and will show BE-like and/or Comptonization features more or less relevant according to the amount of energy dissipated at early and/or late epochs.

2.2 Comparison between observations and models

We compare the measures of the CMB absolute temperature, briefly summarized in section 3, with the above models of distorted spectra for one or two heating processes by using a standard χ^2 analysis.

We determine the limits on the amount of energy possibly injected in the cosmic background at arbitrary primordial epochs corresponding to a redshift z_h (or equivalently to y_h). This topic has been discussed in several papers (see, e.g., Burigana et al. 1991b, Nordberg & Smoot 1998). We improve here the previous methods of analysis by investigating the possibility of properly combining FIRAS data with longer wavelength measurements and by refining the method of comparison with the theoretical models. We will consider the recent improvement in the calibration of the FIRAS data, that sets the CMB scale temperature to 2.725 ± 0.002 K at 95% CL (Mather et al. 1999). We consider the effect on the estimate of the amount of

energy injected in the CMB at a given epoch introduced by the calibration uncertainty of FIRAS scale temperature when FIRAS data are treated jointly to longer wavelength measures. Thus, we investigate the role of available ground and balloon data compared to the FIRAS measures.

Then, we study the combined effect of two different heating processes that may have distorted the CMB spectrum at different epochs. This case has been also considered in the paper by Nordberg & Smoot 1998, where the CMB absolute temperature data are compared with theoretical spectra distorted by a first heating process at $y_h = 5$, a second one at $y_h \ll 1$ and by free-free emission, to derive limits on the parameters that describe these processes. We extend their analysis by considering the full range of epochs for the early and intermediate energy injection process, by taking advantage of the analytical representation of spectral distortions at intermediate redshifts (Burigana et al. 1995). Also in this case, the analysis is performed by taking into account the FIRAS calibration uncertainty.

In each case, we fit the CMB spectrum data for three different values, 0.01, 0.05 and 0.1, of the baryon density $\hat{\Omega}_b$. In presence of an early distortion, $\hat{\Omega}_b$ could be in principle estimated by CMB spectrum observations at long wavelengths, able to detect the wavelength of the minimum of the absolute temperature, determined only by the well known physics of the radiation processes in an expanding universe during the radiation dominated era.

We present our results on the above arguments in section 4.

Then, we extend in section 5 the limits on $\Delta\epsilon/\epsilon_i$ for energy injection processes possibly occurred at $z_h > z_1$, being z_1 is the redshift corresponding to $y_h = 5$, when the Compton scattering was able to restore the kinetic equilibrium between matter and radiation on timescales much shorter than the expansion time and the evolution on the CMB spectrum can be easily studied by replacing the full Kompaneets equation with the differential equations for the evolution of the electron temperature and the chemical potential. This study can be performed by using the simple analytical expressions by Burigana et al. 1991b instead of numerical solutions. For simplicity, we restrict this analysis to the case $\hat{\Omega}_b = 0.05$ and to the best-fit value of the FIRAS calibration.

The relationship between the free-free distortion and the Comptonization distortion produced by late dissipation processes depends on the details of the thermal history at late epochs (Danese & Burigana 1993, Burigana et al. 1995) and can not simply represented by integral parameters. In addition, free-free distortions are particularly important at very long wavelengths, where the measurements have the largest error bars, at least for energy injection processes which give positive distortion parameters; for cooling processes, which generate negative distortion parameters, the effect may be more relevant also at centimetric wavelengths, but the connection between free-free and Comptonization distortions becomes even more crucial. Therefore, we firstly carry out the above analyses of early/intermediate and late distortions by neglecting free-free distortions, i.e. assuming a null free-free distortion parameter y_B . This kind of distortion as well as its impact on the constraints derived for the energy injected at different cosmic times is considered in section 6.

For sake of completeness, we finally observe that negative distortion parameters can be produced by physical processes (e.g., cooling processes, radiative decays of massive particles) that in general are described by a set of process parameters more complex than that considered here (epoch and energy exchange only) and produce spectral shapes different than those considered here. Therefore, the constraints derived for negative values of $\Delta\epsilon/\epsilon_i$ and y_B have to be considered only as indicative.

For compactness, we avoid to report in sections 4 and 6 the fit results for T_0 which is found to be only just different from the FIRAS calibration temperature scale, according to the considered data set and fit parameters. On the contrary, in section 7, where we analyse the implications of the FIRAS calibration as revised by Battistelli et al. 2000, we report also the best fit values found for T_0 in terms of $\Delta T_0 = T_0 - 2.725\text{K}$.

2.3 Sub-millimetric and millimetric foregrounds

A crucial step for the analysis of the CMB spectral distortions is the subtraction of the astrophysical monopole from the total monopole signal. At sub-millimetric wavelengths the integrated contribution from unresolved distant galaxies is expected to significantly overwhelm the difference between the intensities of a distorted spectrum and a blackbody spectrum with the same, or very close, T_0 . This greatly helps the extraction of the sub-millimetric foreground from the total monopole. Three independent methods to extract the sub-millimetric extragalactic monopole from FIRAS data in the “Low” (LLSS, 30–660 GHz) and “High” (RHSS, 60–2880 GHz) frequency bands (see COBE/FIRAS Explanatory Supplement 1995) carried out in the recent past by Puget et al. 1996, Burigana & Popa 1998 and Fixsen et al. 1998 are in good agreement one each other; in particular, the sub-millimetric extragalactic foreground derived by Fixsen et al. 1998 is given by $I_{F98} \simeq 1.3 \times 10^{-5} [\nu/(c/0.01\text{cm})]^{0.64} B_\nu(18.5\text{K})$. These results support a high redshift ($z \simeq 2.1 - 3.8$) active phase of star formation rate and dust reprocessing (Burigana et al. 1997, Sadat et al. 2001). The levels of the sub-millimetric extragalactic foreground theoretically predicted on the basis of the number counts modelled by Franceschini et al. (1994) and revised by Toffolatti et al. (1998) or modelled by Guiderdoni et al. (1998) are in quite good agreement one each other (within a factor ~ 2) and quite consistent with the sub-millimetric extragalactic monopole as derived in the three above works, being respectively only just below or above it (see also, e.g., De Zotti et al. 1999). In addition, the subtraction of the isotropic residual in the FIRAS (LLSS) data as firstly modelled by Fixsen et al. 1996 in terms of a relatively steep spectral form, $I_{F96} \simeq G_0(\nu/\text{Hz})^\beta B_\nu(T_d)$,

being $G_0 \simeq 4.63 \times 10^{-29}$ (Fixsen, private communication), $\beta = 2$ the dust emissivity index and $B_\nu(T_d)$ the brightness of a blackbody at the dust temperature $T_d = 9$ K, does not produce a significant lowering of the upper limits on spectral distortions, as discussed by Burigana et al. 1997. In fact, they found that the allowed ranges for spectral distortion parameters do not change substantially by allowing for somewhat different astrophysical monopole shapes, as in the case of a dust emissivity index varying in the range $1.5 \lesssim \beta \lesssim 2.1$ consistent with the study of cosmic dust grains by Mennella et al. 1998.

On the other hand, Battistelli et al. (2000) recently reconsidered the absolute calibration of the FIRAS data on the basis of numerical simulations of the external calibrator emissivity. As a variance with respect to the previous analysis by Fixsen et al. 1996, they found an emissivity essentially constant within the 0.01% at wavelengths $1 \text{ mm} \gtrsim \lambda \gtrsim 600 \mu\text{m}$, where FIRAS sensitivity is particularly good, and decreasing with the wavelengths of up to about the 0.05% in the range $0.5 \text{ cm} \gtrsim \lambda \gtrsim 1 \text{ mm}$. This translates into a significantly non flat shape of the monopole thermodynamic temperature, after the subtraction of the isotropic astrophysical foreground modelled as discussed above. While a critical discussion of the FIRAS calibration from the experimental point of view is out of the scope of the present work, we consider here the implications of this revised calibration. Being the shape and the level of the sub-millimetric foreground quite well defined both from the observational and the theoretical point of view, this revised FIRAS calibration, significantly non flat at $\lambda \gtrsim 1 \text{ mm}$, should imply larger upper limits on CMB spectral distortion parameters, as suggested by Battistelli et al. 2000, (or even a possible detection of spectral distortions) or a presence of an astrophysical foreground possibly higher than that derived from the extrapolation of the sub-millimetric foreground to wavelengths about or larger than 1 mm, or, finally, a combination of these two effects. We critically discuss these arguments in section 7.

3 THE DATA SETS

For the present study, we have extracted five different sets of measures. Four of them have been chosen to take advantage from the very accurate informations from the FIRAS instrument aboard the COBE satellite. In particular, we considered that the statistical error associated to the measure at any channel of FIRAS is very small (0.02÷0.2 mK, Fixsen et al. 1996) and that the scale temperature at which the FIRAS data are set, have a systematic uncertainty of 2 mK at 95% CL given by the calibration uncertainty (Mather et al. 1999). We analyze the impact of the calibration uncertainty in the determination of the amount of the energy injected in the cosmic background, when the FIRAS measures are considered together with the data from ground and balloon experiments. Thus, we combine a set (see Table 1) of recent CMB spectrum data extracted from the complete database of CMB absolute temperature currently available at the different wavelengths (see, e.g., Salvaterra & Burigana 2000) with the FIRAS data calibrated at the best-fit value as well as at the upper and lower limit (at 95% CL) of the temperature calibration. Finally, we separately consider in the last set of data all the ground and balloon-borne measures reported in Table 1.

In the set of measures we do not include those from the COBRA experiment nor those based on the analysis of the molecular lines, falling these experiments in the same frequency range of the much more accurate FIRAS measures.

Summing up, we exploit five different data sets.

Data set 1): the FIRAS data alone (47 data points); the residuals reported in Table 4 of Fixsen et al. 1996 are added to a blackbody calibrated at the most recent value of 2.725 K (Mather et al. 1999) and only the statistical errors channel by channel (see the uncertainties reported in Table 4 of Fixsen et al. 1996) are taken into account. These data are completed by adding four points at 2.735 K (Mather et al. 1990) in the range $1 < \nu < 2 \text{ cm}^{-1}$ with a systematic error of 0.060 K, discarded in the following calibrations of the scale temperature.

Data set 2): the data of Table 1 of the last two decades and the FIRAS data as above, i.e. calibrated at 2.725 K.

Data set 3): the data of Table 1 of the last two decades and the FIRAS data as above but calibrated at the lower calibration limit (2.723 K, 95% CL).

Data set 4): the data of Table 1 of the last two decades and the FIRAS data as above but calibrated at the upper calibration limit (2.727 K, 95% CL).

Data set 5): all the data of Table 1.

In this way, we analyze in the three cases (2, 3, 4) the impact of the FIRAS data calibration in the determination of the amount of the energy possibly injected in the radiation field without losing the important spectral shape informations provided by the small statistical errors in the channel by channel measures.

The comparison of the results obtained in the last case with those obtained in the other cases allows to understand the different roles of ground and balloon-borne measures and of the FIRAS data. In some cases, we complete this analysis by considering other different combination of FIRAS data and long wavelength measures (see sections 4.1.2 and 6).

ν (GHz)	λ (cm)	T_{th} (K)	Error (K)	Reference
0.408	73.5	3.7	1.2	Howell & Shakeshaft 1967
0.610	49.1	3.7	1.2	Howell & Shakeshaft 1967
0.635	47.2	3.0	0.5	Stankevich et al. 1970
1	30	2.5	0.3	Pelyushenko & Stankevich 1969
1.42	21.2	3.2	1.0	Penzias & Wilson 1967
1.44	20.9	2.5	0.3	Pelyushenko & Stankevich 1969
1.45	20.7	2.8	0.6	Howell & Shakeshaft 1966
2	15	2.5	0.3	Pelyushenko & Stankevich 1969
2.3	13.1	2.66	0.7	Otoshi & Stelzreid 1975
4.08	7.35	3.5	1.0	Penzias & Wilson, 1965
9.4	3.2	3.0	0.5	Roll & Wilkinson 1966
9.4	3.2	2.69	+0.16/ - 0.21	Stokes et al. 1967
19.0	1.58	2.78	+0.12/ - 0.17	Stokes et al. 1967
20	1.5	2.0	0.4	Welch et al 1967
32.5	0.924	3.16	0.26	Ewing et al. 1967
35.0	0.856	2.56	+0.17/ - 0.22	Wilkinson 1967
37	0.82	2.9	0.7	Puzanov et al. 1968
83.8	0.358	2.4	0.7	Kislyakov et al. 1971
90	0.33	2.46	+0.40/ - 0.44	Boynton et al. 1968
90	0.33	2.61	0.25	Millea et al. 1971
90	0.33	2.48	0.54	Boynton & Stokes 1974
0.6	50.0	3.0	1.2	Sironi et al. 1990
0.82	36.6	2.7	1.6	Sironi et al. 1991
1.28	23.3	3.45	0.78	Raghunathan & Subrahmanyan 2000
1.4	21.3	2.11	0.38	Levin et al. 1988
1.43	21	2.65	+0.33/ - 0.30	Staggs et al. 1996a
1.47	20.4	2.27	0.19	Bensadoun et al. 1993
2	15	2.55	0.14	Bersanelli et al. 1994
2.5	12	2.71	0.21	Sironi et al. 1991
3.8	7.9	2.64	0.06	De Amici et al. 1991
4.75	6.3	2.7	0.07	Mandolesi et al. 1986
7.5	4.0	2.6	0.07	Kogut et al. 1990
7.5	4.0	2.64	0.06	Levin et al. 1992
10	3	2.62	0.058	Kogut et al. 1988
10.7	2.8	2.730	0.014	Staggs et al. 1996b
24.8	1.2	2.783	0.089	Johnson & Wilkinson 1987
33	0.909	2.81	0.12	De Amici et al. 1985
90	0.33	2.60	0.09	Bersanelli et al. 1989
90	0.33	2.712	0.020	Schuster 1993.

Table 1. Measures of the absolute thermodynamic temperature of CMB spectrum considered in this work in addition to the COBE/FIRAS data. We separately report the data of the first two decades and of the last two decades since the CMB discovery.

4 RESULTS

The fits are based on the χ^2 analysis, carried out with a specific code based on the MINUIT package of the CERN library (<http://cern.web.cern.ch/CERN/>) and on the set of subroutines and functions that implements the semi-analytical description of the CMB distorted spectra by Burigana et al. 1995. Our code allows to compare the CMB distorted spectrum models with the observational data without the necessity of interpolating frames of numerical solutions (as in Burigana et al. 1991b) and to make the computation much more faster without any significant loss of accuracy, given the very good agreement between the semi-analytical expressions and the numerical solutions.

The CMB spectrum data are compared with the theoretical models by using the MINUIT minimization routines (see the MINUIT/CERN documentation for further details). The physical parameters that describe the distorted spectrum, can be set by choosing on which ones to have the fit. A more detailed description of our code can be found in Burigana & Salvaterra 2000.

We fit the different data sets with a distorted spectrum for different values of the dimensionless time parameter y_h ($y_h = 5, 4, 3, 2, 1, 0.5, 0.25, 0.1, 0.05, 0.025, 0.01$ and $\ll 1$) in order to determine the value and the relative uncertainty of the present radiation temperature, T_0 , and of the fractional energy, $\Delta\epsilon/\epsilon_i$. [Of course, the redshift z_h corresponding to a given value of y_h decreases with the increase of baryon density (see eq. 2); for graphic purposes, we report in the plots the exact values of y_h and the power law approximation $z_h(y_h) \simeq 4.94 \times 10^4 y_h^{0.477} \hat{\Omega}_b^{-0.473}$ (Burigana et al. 1991b) for the redshift.]

4.1 Fits with a single energy injection

In this section we present the results of the fits to the five data sets described in section 3 with spectra distorted by a single energy injection.

4.1.1 Including FIRAS data

The results obtained for the data set 1) (FIRAS data only) are shown in Fig. 1 for the full set of y_h and the representative case $\hat{\Omega}_b = 0.05$. By comparing the results obtained for $\hat{\Omega}_b = 0.01$ and 0.1 we find that the baryon density does not influence the limits on $\Delta\epsilon/\epsilon_i$ derived from current data for cosmic epochs corresponding to the same dimensionless time y_h of dissipation epoch, although the redshift corresponding to the same y_h decreases with the baryon density.

The results are always compatible with null values of the distortion parameters, the best fit values of $\Delta\epsilon/\epsilon_i$ being only just different from zero. The χ^2 best fit value does not change significantly with y_h and $\hat{\Omega}_b$, being the χ^2/DOF very close to unit; therefore this data do not show a favourite epoch for a possible (very small) energy injection nor provide informations on the baryon density. On the other hand, the limits on $\Delta\epsilon/\epsilon_i$ significantly depend on the epoch of the energy injection, being about a factor two larger for early than for late dissipation processes; this is clearly related to the range of frequencies observed by FIRAS.

In principle, the measures at centimetric and decimetric wavelengths could play a crucial role to investigate on the presence of early distortions, due to the large decrease of the CMB absolute temperature in the Rayleigh-Jeans region. The results found for the data set 2) (recent data and FIRAS data calibrated at 2.725 K) and $\hat{\Omega}_b = 0.05$ are shown in Fig. 1; again, we find results essentially independent of the baryon density, in spite the fact that the available ground observations cover also the long wavelength spectral region where the amplitude of possible early distortions strongly depend on $\hat{\Omega}_b$. In general, as evident from the comparison with the results based on the data set 1), the ground and balloon data do not change significantly the constraints on energy dissipations with respect to the FIRAS measures alone, independently of the considered energy injection epoch, because of their large error bars.

Even considering the full range of frequencies, it is impossible to determine a favourite energy injection epoch or a favourite baryon density value, as indicated by the χ^2 values, substantially constant with y_h and $\hat{\Omega}_b$. The χ^2/DOF (~ 1.1) is only just larger than that obtained in the case of the data set 1). This weak increase of the χ^2/DOF is due to the well known disagreement between the absolute temperature of the FIRAS data and the averaged temperature of the data at $\lambda \gtrsim 1$ cm.

We have analyzed also the impact of the calibration uncertainty (2 mK at 95% CL, Mather et al. 1999) in the FIRAS data combined with the recent measures at $\lambda \gtrsim 1$ cm (data set 3) and data set 4): we find a negligible impact on the fit results. By assuming the lowest FIRAS calibration only a small improvement (of $\sim 2\%$) in the χ^2/DOF is found with respect to the case of the highest calibration, as expected since the lower averaged temperature value at $\lambda \gtrsim 1$ cm than at $\lambda \lesssim 1$ cm. Thus, our analysis demonstrate that the current constraints on the energy possibly injected in the cosmic radiation field are essentially set by the FIRAS measures alone independently of the cosmic epoch.

Finally, we report in Table 2 (rows 1–4) the values of best-fit of the fractional injected energy, $\Delta\epsilon/\epsilon_i$, in the case of a heating process at early ($y_h = 5$, BE like spectrum) and late ($y_h \ll 1$, Comptonized spectrum) epochs, with the corresponding uncertainties.

4.1.2 Neglecting FIRAS data

The results obtained for the data set 5) (all the data of Table 1 without including FIRAS data) are shown in Fig. 2 for the full set of y_h and the representative case $\hat{\Omega}_b = 0.05$.

In this case the best fit values of $\Delta\epsilon/\epsilon_i$ for early processes ($y_h \gtrsim 2$), although compatible with a BB spectrum at about 2σ level, are significantly (at about 1σ level) positive, ranging from $\simeq 1.4 \times 10^{-3}$ to $\simeq 2 \times 10^{-3}$ for $5 \gtrsim y_h \gtrsim 2$. On the contrary, from this long wavelength set of data it is no longer possible to tightly constrain dissipation processes at $y_h \lesssim 1$.

We find a χ^2 best fit value slightly decreasing with y_h . We find also a weak, but not completely negligible, dependence of $\Delta\epsilon/\epsilon_i$ on $\hat{\Omega}_b$: for example, for $\hat{\Omega}_b = 0.01$ ($\hat{\Omega}_b = 0.1$) the (95% CL) upper limit on $\Delta\epsilon/\epsilon_i$ decreases (increases) of about 1.5% (14%) with respect to upper limit obtained for $\hat{\Omega}_b = 0.05$.

We report in Table 2 (row 5) the values of best-fit of the fractional injected energy, $\Delta\epsilon/\epsilon_i$, in the case of a heating process at early ($y_h = 5$, BE like spectrum) and late ($y_h \ll 1$, Comptonized spectrum) epochs, with the corresponding uncertainties at 95% CL.

Finally, we note that these results are mainly driven by the observations of the last two decades. In fact, by considering only these measures we obtain $(\Delta\epsilon/\epsilon_i)/10^{-5} = (1.57 \pm 1.45) \times 10^2$ and $(\Delta\epsilon/\epsilon_i)/10^{-5} = [-0.10(+1.93/-1.49)] \times 10^4$ respectively in the case of an early ($y_h = 5$, BE like spectrum) and a late ($y_h \ll 1$, Comptonized spectrum) process (errors at 95% CL).

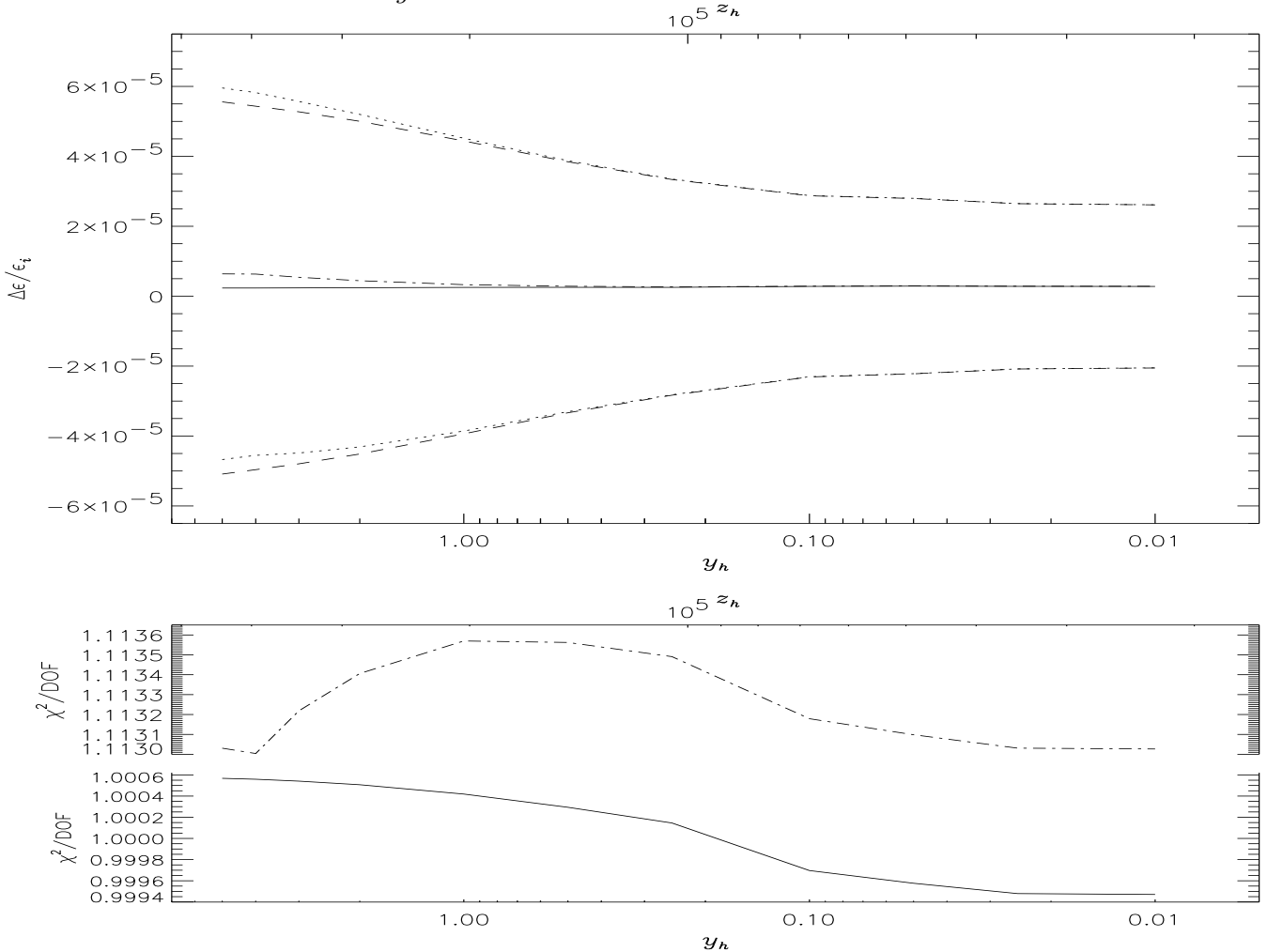


Figure 1. Top panel: best fit and constraints at 95% CL on $\Delta\epsilon/\epsilon_i$ as function of the energy dissipation epoch in the case on a single process occurred in the thermal history of the universe. Bottom panel: values of the χ^2/DOF corresponding to the best fit curves. We show here the results obtained from the data set 1) (solid lines - best fit - and dashed lines - upper and lower limits) and the data set 2) (dot-dashed lines and dotted lines). Note how current ground and balloon measures do not significantly modify the constraints on $\Delta\epsilon/\epsilon_i$ derived from the FIRAS data alone, while the χ^2/DOF increases of about 0.11 [$\hat{\Omega}_b = 0.05$].

4.2 Fits with two energy injections

We analyse here the constraints set by the available measures when we take into account the possibility that two heating processes could have distorted the CMB spectrum at different epochs, early or intermediate for the former and late for the latter. More explicitly, we obtain the limits on the amount of the first energy injection for each value of y_h (in the range $5 \geq y_h \geq 0.01$) under the hypothesis of a possible existence of a second late heating (at $y_h \ll 1$) and on the amount of the second late energy injection (at $y_h \ll 1$) under the hypothesis of a possible existence of an earlier energy dissipation occurring at different values of y_h (in the range $5 \geq y_h \geq 0.01$). So far, we extend the analysis of Nordberg & Smoot 1998 which considered only the case of an early dissipation at $y_h = 5$ combined with a late one at $y_h \ll 1$. Our results are then clearly comparable to those obtained in the section 4.1: we expect that, by including the possibility of two heating processes at different cosmic epochs, the constraints on $\Delta\epsilon/\epsilon_i$, both for early and late processes, are relaxed with respect to the case in which a single heating in the thermal history of the universe is considered.

Of course, it is particularly interesting in this context to exploit the whole frequency range of the recent CMB spectrum measures [i.e. the data set 2), 3), and 4)]. For comparison, in the exploitation of the data set 1) we circumscribe our joint analysis just to the simple circumstance of two processes at $y_h = 5$ and $y_h \ll 1$ (see Table 3), while neglecting FIRAS data makes this analysis meaningless, as evident from the results of section 4.1.2 in the case of late distortions.

We report here in detail the results obtained by exploiting the data set 2) for $\hat{\Omega}_b = 0.05$ (see Fig. 3); again, the constraints on the energy dissipated at different epochs are essentially independent of the baryon density when expressed in terms of the dimensionless time y_h . The top panel of Fig. 3 shows the best fit value of the fractional energy exchanged in the plasma as a function of the cosmic epoch (for $5 \gtrsim y_h \gtrsim 0.01$) and its upper and lower limits at 95% CL when we allow for a possible later

Data set	$(\Delta\epsilon/\epsilon_i)/10^{-5}$		$y_B/10^{-5}$
	heating at $y_h = 5$	heating at $y_h \ll 1$	
set 1): FIRAS	0.23 ± 5.33	0.28 ± 2.33	2.72 ± 9.20
set 2): Table 1 (1985-2000) + FIRAS (2.725 K)	0.64 ± 5.32	0.28 ± 2.33	-4.55 ± 4.24
set 3): Table 1 (1985-2000) + FIRAS (2.723 K)	0.63 ± 5.33	0.29 ± 2.34	-4.46 ± 4.25
set 4): Table 1 (1985-2000) + FIRAS (2.727 K)	0.66 ± 5.31	0.29 ± 2.33	-4.64 ± 4.23
set 5): Table 1	$(1.36 \pm 1.32) \times 10^2$	$[-0.14(+1.90/-1.47)] \times 10^4$	-0.63 ± 2.44

Table 2. Results on the energy injected at $y_h = 5$ and at $y_h \ll 1$ and on the free-free distortion parameter y_B . Fits to the different data sets, errors at 95% CL. We jointly fit two parameters, T_0 and the $(\Delta\epsilon/\epsilon_i)$ referring to the early or late process or y_B , by assuming null values for the other distortion parameters [$\widehat{\Omega}_b = 0.05$].

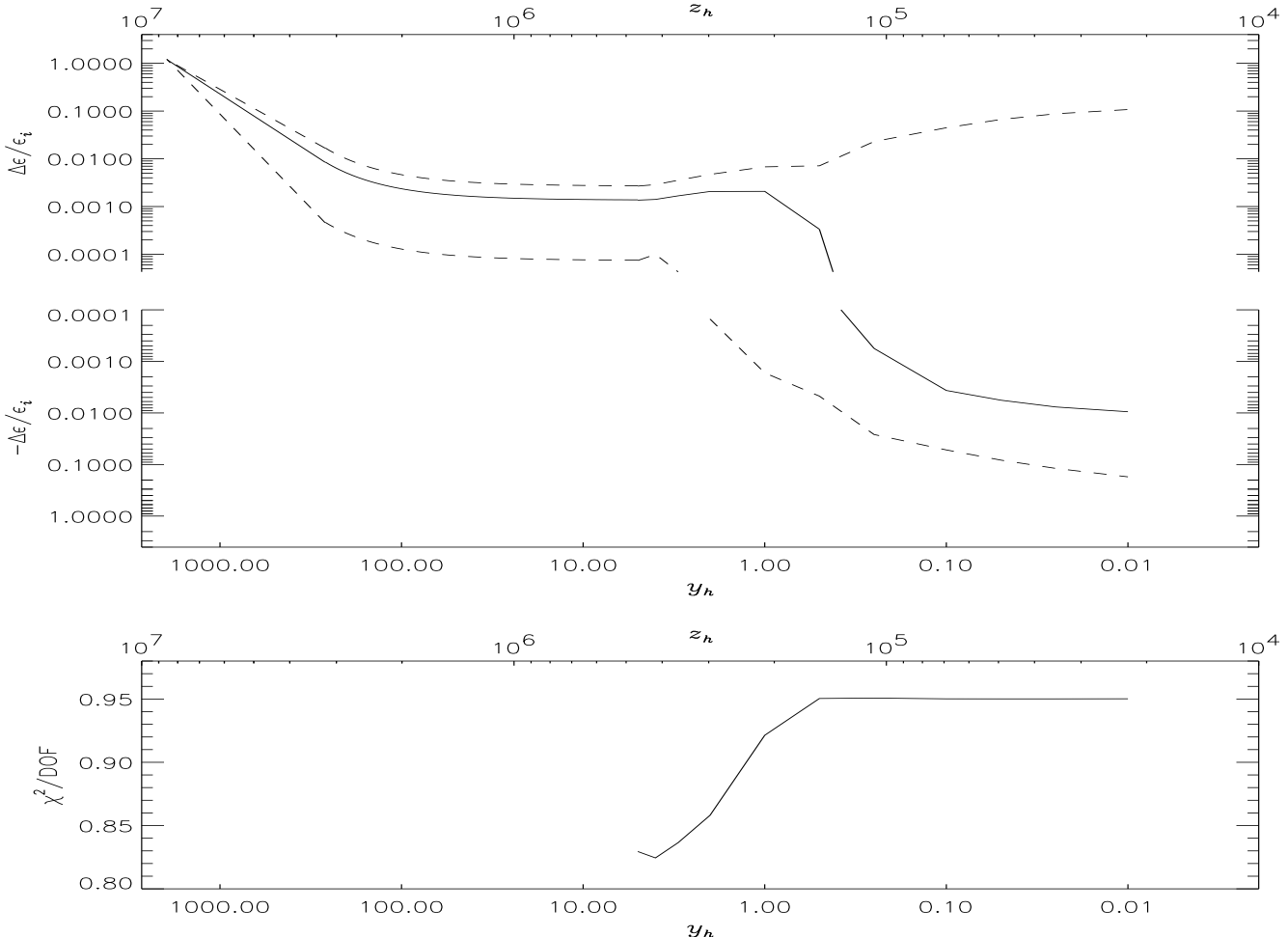


Figure 2. The same as in Fig. 1, but by exploiting all the data of Table 1 and neglecting the FIRAS data. We report here also the constraints on the energy exchange at very high redshifts, as described in section 5, for comparison with the results shown in Fig. 4. Of course, the constraints on $\Delta\epsilon/\epsilon_i$ obtained by neglecting FIRAS data are significantly relaxed at each cosmic epoch [$\widehat{\Omega}_b = 0.05$].

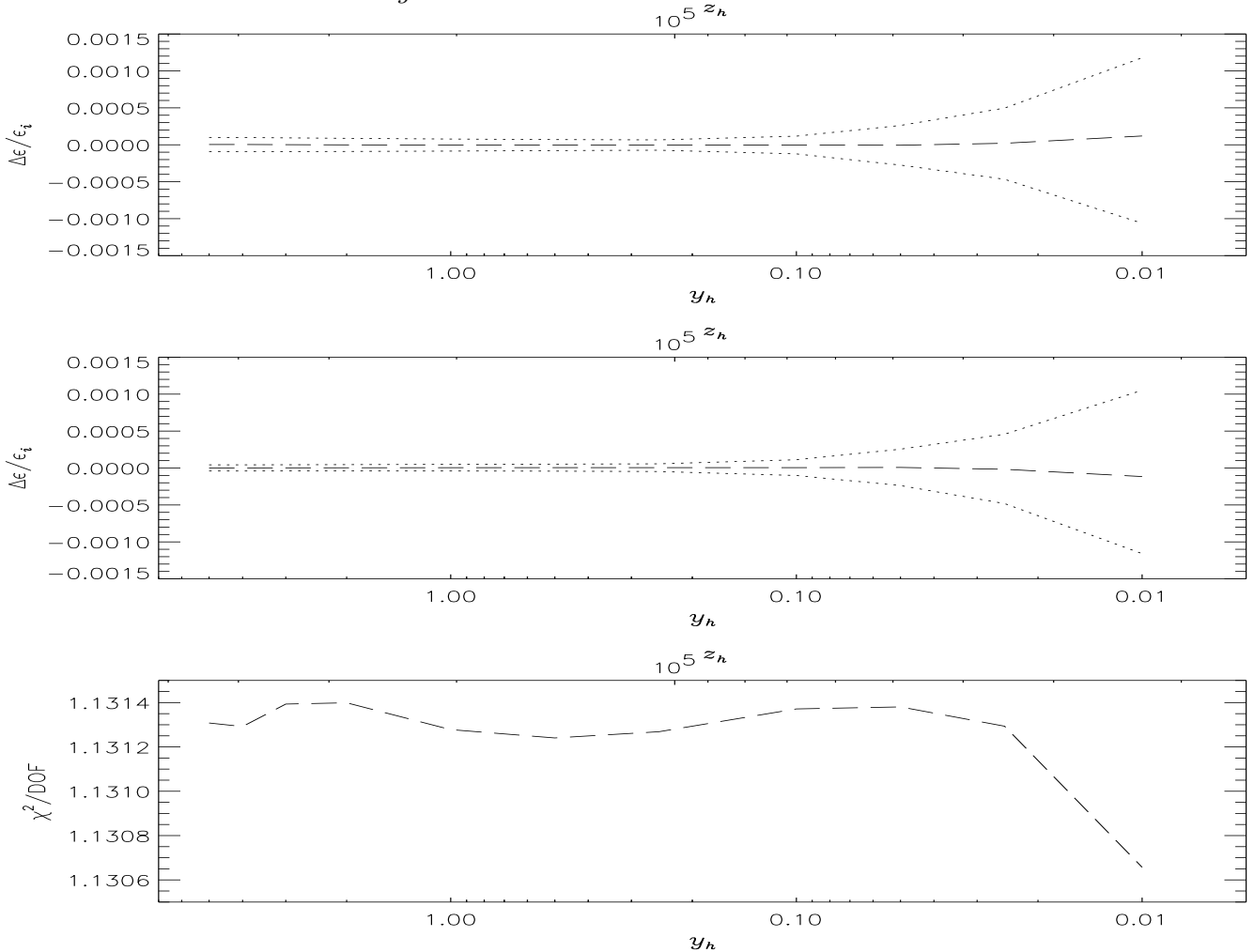


Figure 3. Top panel: best fit (long dashes) and constraints (dotted lines) at 95% CL on the earlier ($y_h \gtrsim 0.01$) energy exchange, $\Delta\epsilon/\epsilon_i$, as function of the dissipation epoch when we allow also for a late ($y_h \ll 1$) energy exchange in the thermal history of the universe. Middle panel: best fit and constraints at 95% CL on the late ($y_h \ll 1$) energy exchange, $\Delta\epsilon/\epsilon_i$, as function of the dissipation epoch of an earlier ($y_h \gtrsim 0.01$) energy exchange occurring at a given epoch in the thermal history of the universe. Bottom panel: values of the χ^2/DOF corresponding to the best fit curves. We show here the results obtained by exploiting the data set 2) [$\widehat{\Omega}_b = 0.05$].

dissipation process ($y_h \ll 1$). The middle panel reports the best fit value of the fractional energy exchanged in the plasma at $y_h \ll 1$ and its upper and lower limits when we allow for a possible earlier dissipation process (occurring at $5 \gtrsim y_h \gtrsim 0.01$). The bottom panel gives the χ^2/DOF corresponding to the best fit model obtained by allowing for a late dissipation and an earlier dissipation at a certain epoch y_h ($5 \gtrsim y_h \gtrsim 0.01$).

We note here that, in general, the joint analysis of two dissipation processes results to be meaningless for earlier processes occurring at $y_h < 0.1$ (when the limits on the amount of injected energy became very relaxed), because the imprints produced by a positive (negative) earlier distortion at any $y_h < 0.1$ can be partially compensated by those produced by a later negative (positive) distortion at $y_h \ll 1$ (and this cancellation effect increases for an earlier distortion occurring at smaller and smaller y_h), owing to the similarity of the distorted spectral shapes at small y_h .

As shown by the values reported in Table 3 for the case of a joint analysis of a heating process at $y_h = 5$ and one at $y_h \ll 1$, the limits on $\Delta\epsilon/\epsilon_i$ are relaxed by a factor ~ 2 with respect to the case of in which a single energy injection in the thermal history is considered, both for early and late dissipation processes (see Table 2 for comparison).

Finally, the exact FIRAS calibration returns to be not crucial in the exploitation of current data and the χ^2/DOF value is substantially constant, and close to unit, for the different values of y_h and $\widehat{\Omega}_b$.

Data set	$(\Delta\epsilon/\epsilon_i)/10^{-5}$	
	heating at $y_h = 5$	heating at $y_h \ll 1$
<i>set 1</i>): FIRAS	0.95 ± 9.67	0.61 ± 4.18
<i>set 2</i>): Table 1 (1985-2000) + FIRAS (2.725 K)	0.37 ± 9.62	0.14 ± 4.17
<i>set 3</i>): Table 1 (1985-2000) + FIRAS (2.723 K)	0.27 ± 9.65	0.19 ± 4.19
<i>set 4</i>): Table 1 (1985-2000) + FIRAS (2.727 K)	0.42 ± 9.61	0.12 ± 4.17

Table 3. Results on the energy injected at $y_h = 5$ and $y_h \ll 1$ when these two dissipation processes are jointly considered. Fits to the different data sets, errors at 95% CL. We jointly fit three parameters: T_0 and the two values of $(\Delta\epsilon/\epsilon_i)$ referring to the early and late process [$\hat{\Omega}_b = 0.05$].

5 CONSTRAINTS ON ENERGY INJECTIONS AT VERY HIGH REDSHIFTS

For $z > z_1$ (i.e. $y_h > 5$) the Compton scattering is able, after an energy injection, to restore the kinetic equilibrium between matter and radiation yielding a BE spectrum on timescales smaller than the expansion time, while radiative Compton and Bremsstrahlung work to restore the thermodynamic equilibrium yielding a BB spectrum. Thus, a larger amount of energy would have been needed to yield the same observational effect produced by a dissipation processes at $\sim z_1$. The analytic approximations of Burigana et al. 1991b of the numerical computations carried out by Burigana et al. 1991a,b permits us to extend the limits on $\Delta\epsilon/\epsilon_i$ at $z_h > z_1$ with good accuracy without the necessity of numerical integrations of the chemical potential and electron temperature evolution equations. We have reported here, for simplicity, only the results for $\Delta\epsilon/\epsilon_i(y_h)$ in the case $\hat{\Omega}_b = 0.05$, but analogous constraints can be easily derived for any value of $\hat{\Omega}_b$.

The limits on $\Delta\epsilon/\epsilon_i$ at 95% CL obtained from the accurate measures of FIRAS data alone [data set 1)] and from the recent measures from ground and balloon combined with the FIRAS data calibrated at 2.725 K [data set 2)] are very close one each other (see Fig. 4), in strict analogy with the corresponding limits on the amount of energy injected at $z = z_1$. The FIRAS data significantly constrain the value of $\Delta\epsilon/\epsilon_i$ also at $z > z_1$; of course, a very large energy dissipation at $z \approx z_{therm}$ can not be excluded from CMB spectrum observations. The limits on the energy possibly injected in the radiation field at $z \gtrsim z_{therm}$ can be set by primordial nucleosynthesis analyses.

We obtain also the limits on $\Delta\epsilon/\epsilon_i$ at high z by allowing for a second heating possibly occurred at low z (see again Fig. 4). In this case, the limits at 95% CL on the amount of the energy injected at $z = z_1$, relaxed compared to the case of a single heating in the thermal history of the universe, allow for larger energy dissipations (by a factor up to ~ 2), particularly at $z_1 \lesssim z \lesssim z_{therm}/2$.

Finally, by neglecting FIRAS data and keeping all the data of Table 1 [data set 5)], the constraints on $\Delta\epsilon/\epsilon_i$ result to be much less stringent at each cosmic epoch, as shown in Fig. 2 for the case of a single energy exchange in the thermal history of the universe.

6 FREE-FREE DISTORTIONS

As discussed in section 3.2, a proper joint analysis of Comptonization and free-free distortions requires the specification of the kind of considered thermal history at late epochs.

On the other hand, it is also interesting to evaluate the constraints set by current observations on free-free distortions and the possible impact of free-free distortions on the estimation of the other distortion parameters.

In the last column of Table 2 we report the best fit results and the limits on y_B derived by performing the fit to the different data sets for T_0 and y_B under the assumption of negligible energy exchanges ($\Delta\epsilon/\epsilon_i = 0$ at any y_h). By varying the data from the *set 1*) to the *set 4*), the χ^2/DOF assumes the values $\simeq 0.993, 1.040, 1.045$ and 1.035 . It is also evident from the table the inconsistency at $\simeq 1\sigma$ level between the results based on FIRAS data alone and on the data set including also the recent measures at longer wavelengths. We note also that, on the contrary, the limits on y_B based on all the data of Table 1 alone are consistent with those based on FIRAS data alone. The limits on free-free distortions based on all the data of Table 1 are in fact different from those derived considering only the data of the two last decades ($y_B/10^{-5} = -5.49 \pm 4.92$). This is

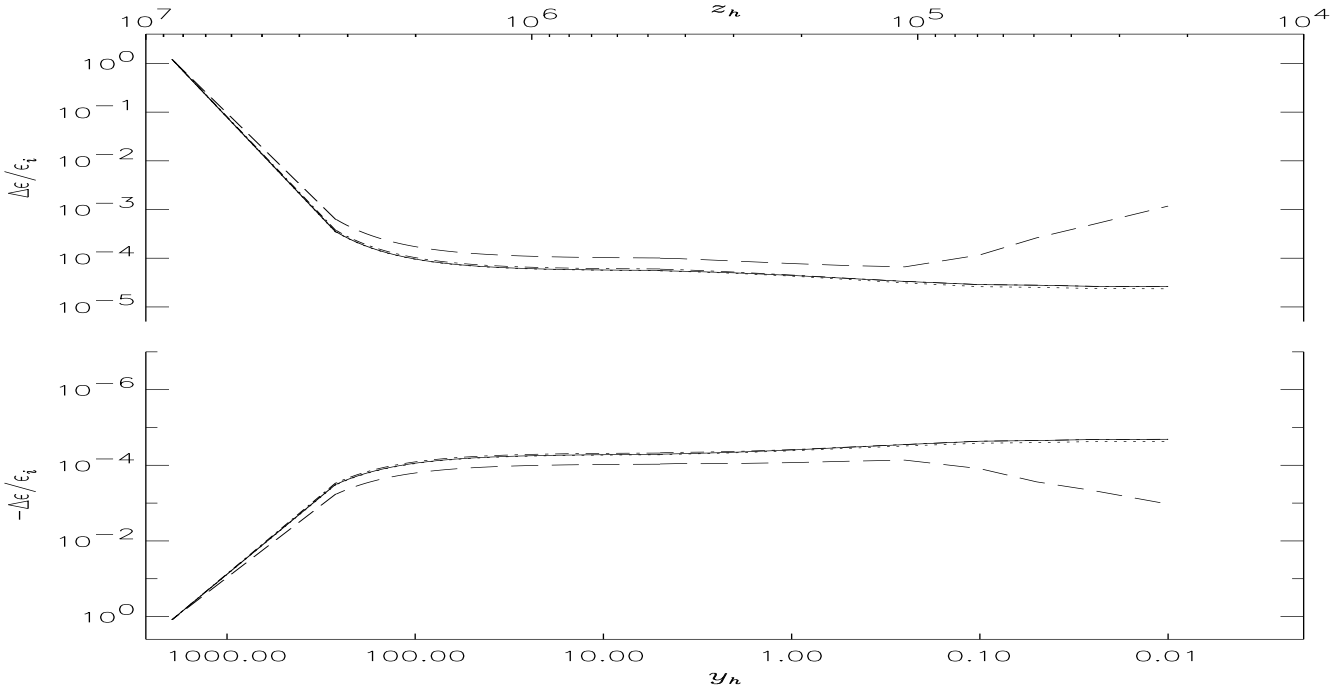


Figure 4. Extension to very high redshifts of the constraints at 95% CL on the energy exchange, $\Delta\epsilon/\epsilon_i$, as function of the dissipation epoch. We consider here several cases: the constraints on a single energy injection in the thermal history of the universe by exploiting the data set 1) (solid lines) and the data set 2) (dot-dashed lines); the constraints on the earlier ($y_h \gtrsim 0.01$) energy exchange, $\Delta\epsilon/\epsilon_i$, when we allow also for a late ($y_h \ll 1$) energy exchange in the thermal history of the universe and exploit the data set 2) (dashed lines). We report also the constraints in the case of a single energy injection in the thermal history of the universe when we exploit the FIRAS data alone but calibrated according to Battistelli et al. (2000) by adding the “experimental” astrophysical monopole, I_{F96} , derived by Fixsen et al. (1996) and subtracting the “theoretical” astrophysical monopole of the best fit obtained assuming a power law plus a dust emission law (dotted lines) as in Table 14. Exploiting different data sets, including FIRAS data, does not change significantly the result, as evident from the superposition of the curves referring to the different cases; this is true also in the case of the calibration by Battistelli et al. (2000) provided that the astrophysical component is properly modelled (see section 7). The only relevant difference appears when we consider a single or a double energy exchange in the thermal history of the universe [$\tilde{\Omega}_b = 0.05$].

mainly due to the measures by Levin et al. 1988 and Bensadoun et al. 1993; neglecting them, from the data of the two last decades we find $y_B/10^{-5} = -2.23 \pm 6.10$. [Errors at 95% CL].

The above inconsistency is again present by allowing also for energy exchanges both at high ($y_h = 5$) and low ($y_h \ll 1$) redshifts (see the last column of Table 4). In Table 4 note also that by exploiting the full frequency range of the recent measures to simultaneously fit T_0 , $\Delta\epsilon/\epsilon_i(y_h = 5)$, $\Delta\epsilon/\epsilon_i(y_h \ll 1)$ and y_B the signs of $\Delta\epsilon/\epsilon_i(y_h \ll 1)$ and y_B are close to be inconsistent at $\simeq 1\sigma$ level. Although the value of the χ^2/DOF ($\simeq 1.062$) represents an improvement with respect to the fit reported in the second row of Table 3 ($\chi^2/\text{DOF} \simeq 1.131$), it is difficult from a physical point of view to explain this inconsistency (a precise fine tuning in the late thermal history is required to produce $\Delta\epsilon/\epsilon_i(y_h \ll 1)$ and y_B with different signs). Again, we note that by using FIRAS data together with the recent data of Table 1 without the measures by Levin et al. 1988 and Bensadoun et al. 1993 or together with all the data of Table 1 to jointly fit T_0 , $\Delta\epsilon/\epsilon_i(y_h = 5)$, $\Delta\epsilon/\epsilon_i(y_h \ll 1)$ and y_B this inconsistency disappears (we find, respectively, $(\Delta\epsilon/\epsilon_i(y_h = 5))/10^{-5} = -1.75 \pm 10.83$, $(\Delta\epsilon/\epsilon_i(y_h \ll 1))/10^{-5} = 0.79 \pm 4.40$, $y_B/10^{-5} = -1.84 \pm 5.55$ and $(\Delta\epsilon/\epsilon_i(y_h = 5))/10^{-5} = -0.29 \pm 9.92$, $(\Delta\epsilon/\epsilon_i(y_h \ll 1))/10^{-5} = 0.34 \pm 4.23$, $y_B/10^{-5} = -0.71 \pm 2.37$, errors at 95% CL).

Clearly, more precise observations at long wavelengths are required for a proper evaluation of free-free distortions.

Finally, we note that, in spite of the above inconsistencies, the constraints on $\Delta\epsilon/\epsilon_i(y_h = 5)$ and on $\Delta\epsilon/\epsilon_i(y_h \ll 1)$ are not particularly modified with respect to the results shown in Table 3, where possible free-free distortions are neglected [†]. This is particularly important, because the constraints on many classes of astrophysical processes are typically based on energetic arguments (see, e.g., Platania et al. 2002 for a recent application).

[†] For the data set 1), which not presents the above inconsistency, the upper limits on $\Delta\epsilon/\epsilon_i(y_h \ll 1)$ are only just modified, whereas a positive free-free distortion can be clearly compensated in part by a somewhat larger energy injection at high redshift (compare the first row of Table 3 – $\chi^2/\text{DOF} \simeq 1.021$ – and of Table 4 – $\chi^2/\text{DOF} \simeq 1.029$).

Data set	$(\Delta\epsilon/\epsilon_i)/10^{-5}$		$y_B/10^{-5}$
	heating at $y_h = 5$	heating at $y_h \ll 1$	free-free dist. at $y_h \ll 1$
set 1): FIRAS	4.14 ± 15.61	-0.85 ± 5.46	6.35 ± 15.31
set 2): Table 1 (1985-2000) + FIRAS (2.725 K)	4.65 ± 10.56	1.63 ± 4.36	-5.40 ± 4.69

Table 4. Results on the energy injected at $y_h = 5$ and $y_h \ll 1$ and on the free-free distortion parameter when these three types of distortions are jointly considered. Fits to the different data sets, errors at 95% CL. We jointly fit four parameters: T_0 , the two values of $(\Delta\epsilon/\epsilon_i)$ referring to the early and late process and y_B [$\hat{\Omega}_b = 0.05$].

7 IMPLICATIONS OF A REVISED CALIBRATION OF FIRAS DATA

The calibration of the FIRAS data as function of the frequency (i.e. its spectral shape), particularly in the Low (LLSS) frequency bands, is crucial to probe CMB spectral distortions because of the extremely good sensitivity of FIRAS (~ 0.1 mK, see Fig. 5) at each frequency channel. In the previous sections we have assumed the FIRAS calibration derived by the COBE/FIRAS team as described by Fixsen et al. 1994, Fixsen et al. 1996 and revised by Mather et al. 1999. According to the authors, the external calibrator shows a very low reflectance, ρ , less than 3×10^{-5} at $\lambda = 1$ cm and decreasing with the frequency, and then an emissivity function, $e = 1 - \rho$, very close to unit at each wavelength. Battistelli et al. (2000) have recently reanalysed the emissivity of the calibrator by using numerical simulations based on Ray-Tracing techniques. They find that the relatively small dimension of the inner part of the V-groove could distort the emission spectrum when it becomes comparable with the wavelength. In this condition the diffraction may be relevant in the final reflection. The authors studied this problem by using a waveguide model (“wave radial waveguide”) to compute the emissivity function of the external calibrator under various diffraction configurations.

7.1 The recalibrated data set

According to the results reported in Fig. 12 of Battistelli et al. (2000), the spectrum of the FIRAS calibrator is given by a blackbody (assumed here at a temperature of 2.725 K, according to Mather et al. 1999) multiplied by a frequency dependent emissivity function, e , very close to unit at the highest frequencies but significantly decreasing with the wavelength for $\lambda \gtrsim 0.1$ cm. As stressed by the authors, a completely exhaustive analysis of FIRAS calibration is a very difficult task. The calibration spectral shape may be conservatively considered as varying from the case of constant emissivity (i.e., a pure blackbody shape) to a case of maximum deviation from a blackbody shape which shows an emissivity decrease of about 0.07% at $\lambda \simeq 0.5$ cm. In the former case the measures are substantially equivalent to the data set 1) described in section 3. In the latter case, the revised calibration implies a maximum deviation from the Planckian spectrum. We consider here the cosmological and astrophysical implications of the calibrator emissivity law given by Table 1 of Battistelli et al. 2000 which “represents the conservation of the transmitted flux inside the radiator”. We construct then a new set of CMB absolute temperature (referred as R-FIRAS in the following tables and figure captions) by adding this revised calibration spectrum to the residuals of Table 4 of Fixsen et al. 1996 by assuming the same statistical uncertainties. As evident from Fig. 5, this revised calibration is substantially equivalent to that of Mather et al. 1999 for $\lambda \lesssim 0.1$ cm, but implies a decrement of the CMB absolute temperature of about 1 mK from $\simeq 0.1$ cm to $\simeq 0.5$ cm. This calls for an accuracy of future CMB spectrum measurements about ~ 1 cm better than ~ 1 mK (both in sensitivity and calibration) to clearly distinguish between the two FIRAS data calibration shapes.

In sections 7.2–7.5 we will analyse the FIRAS data so revised without resorting to particular cosmological or astrophysical considerations. We will include them in the discussion of section 7.6.

7.2 Interpretation in terms of pure CMB spectral distortions

We tried to explain this revised FIRAS data set in terms of pure CMB spectral distortions. Our results are summarized in Tables 5, 6 and 7, where we consider separately the case of an early heating process, a late heating process and a free-free distortion with negligible energy exchange, the joint effect of an early and a late dissipation process, and, finally, the joint effect of an early and a late dissipation process associated to a non negligible free-free distortion, respectively. As evident from

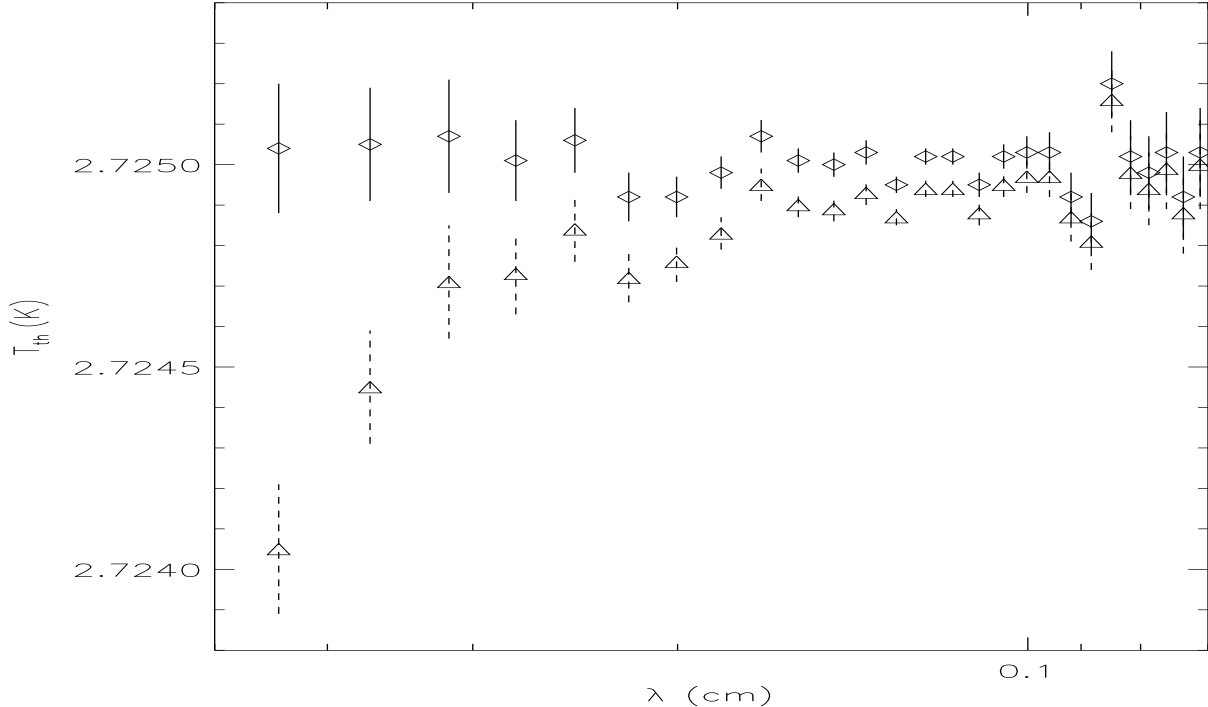


Figure 5. Comparison between the CMB absolute thermodynamic temperatures derived from FIRAS data calibrated according to Mather et al. 1999 (diamonds) and to Battistelli et al. (2000) (triangles) [see also the text].

Data set	$(\Delta\epsilon/\epsilon_i)/10^{-5}$		$y_B/10^{-5}$
	heating at $y_h = 5$	heating at $y_h \ll 1$	
	free-free dist. at $y_h \ll 1$		
R-FIRAS	20.15 ± 5.32	6.07 ± 2.30	-28.71 ± 9.19
$\Delta T_0(\text{K})/10^{-4}$	-1.16 ± 0.16	-0.71 ± 0.17	-0.89 ± 0.15
χ^2/DOF	1.248	1.906	1.657

Table 5. Results on the energy injected at $y_h = 5$ and at $y_h \ll 1$ and on the free-free distortion parameter y_B . Fits to the FIRAS data with the revised calibration, errors at 95% CL. We jointly fit two parameters, T_0 and the $(\Delta\epsilon/\epsilon_i)$ referring to the early or the late process or the parameter y_B , by assuming null values for the other distortion parameters [$\widehat{\Omega}_b = 0.05$].

the fit results, these revised FIRAS data support the existence of an early dissipation process with $\Delta\epsilon/\epsilon_i \sim (0.5 \div 4) \times 10^{-4}$. Comptonization distortions only marginally improve the fit (by reducing of only about the 5% the χ^2/DOF for a late cooling process, compare Tables 6 and 7 with the second column of Table 5). Adding free-free distortions does not improve the fit (compare Table 7 with Table 6). As discussed in section 6, precise long wavelength observations are required to evaluate free-free distortions; we neglect them in the following considerations.

We observe that, in any case, by considering only CMB spectral distortions the value of the χ^2/DOF is always larger than $\simeq 1.2$, even in this favourite case in which a single set of measurements is considered.

7.3 Interpretation in terms of millimetric astrophysical foreground

Given the relatively high χ^2/DOF obtained in the previous section when the revised FIRAS data are interpreted in terms of pure CMB distortions, we investigate here if it is possible to better explain them by supposing the existence of a monopole of

Data set	$(\Delta\epsilon/\epsilon_i)/10^{-5}$	$\Delta T_0(\text{K})/10^{-4}$		χ^2/DOF
	heating at $y_h = 5$	heating at $y_h \ll 1$		
R-FIRAS	27.83 ± 9.66	-3.99 ± 4.18	-1.40 ± 0.29	1.194

Table 6. Results on the energy injected at $y_h = 5$ and at $y_h \ll 1$ by assuming a null free-free distortion parameter y_B . Fits to the FIRAS data with the revised calibration, errors at 95% CL. We jointly fit three parameters: T_0 and the two $(\Delta\epsilon/\epsilon_i)$ values referring to the early and the late process [$\widehat{\Omega}_b = 0.05$].

Data set	$(\Delta\epsilon/\epsilon_i)/10^{-5}$	$y_B/10^{-5}$	$\Delta T_0(\text{K})/10^{-4}$	χ^2/DOF	
	heating at $y_h = 5$	heating at $y_h \ll 1$	free-free dist. at $y_h \ll 1$		
R-FIRAS	21.86 ± 15.62	-2.27 ± 5.46	-7.45 ± 15.30	-1.25 ± 0.42	1.200

Table 7. Results on the energy injected at $y_h = 5$ and at $y_h \ll 1$ and on the free-free distortion parameter y_B . Fits to the FIRAS data with the revised calibration, errors at 95% CL. We jointly fit four parameters: T_0 , the two $(\Delta\epsilon/\epsilon_i)$ values referring to the early and the late process and y_B [$\widehat{\Omega}_b = 0.05$].

astrophysical nature not subtracted in the data reduction with a significant contribution at millimetric wavelengths. We try a fit in terms of a power law, $I_{PL} = k(\lambda/\text{cm})^{-\alpha}$, and in terms of a dust emission law approximated by a modified blackbody, $I_D = k_d(\lambda/\text{cm})^{-\beta-3}/[\exp(h\nu/kT_d) - 1]$; we report the following fit results in terms of $\log k$ and $\log k_d$ with k and k_d expressed in units of $\text{erg cm}^{-2}\text{sec}^{-1}\text{sr}^{-1}\text{Hz}^{-1}$.

The fit results are reported in Tables 8 and 9. As evident, a single modified blackbody component provides a somewhat better fit than a combination of two or three CMB spectral distortions. Although described by three parameters, as in the case of Table 7, the interpretation of these data in terms of a single dust emission law at a temperature only just above that of the CMB seems to be easier than a proper combination of two dissipation processes at different cosmic epochs, but in any case the χ^2/DOF , of about 1.2, still remains significantly higher than unit.

7.4 Readding the sub-millimetric foreground

As discussed in the previous subsections, the FIRAS data recalibrated according to Battistelli et al. 2000 can not be fully explained in terms of CMB distortions or of an additional astrophysical component. On the other hand, we have carried out this analysis by assuming the same subtraction to the (LLSS) FIRAS monopole of the astrophysical monopole, I_{F96} , derived by Fixsen et al. 1996 which is clearly appropriate in the case of a FIRAS calibration with an emissivity function very close to unit in the whole LLSS range.

Data set	$\Delta T_0(\text{K})/10^{-4}$	$\log k$	α	χ^2/DOF
R-FIRAS	-1.10 ± 0.26	-20.49 ± 1.90	1.39 ± 1.50	2.398

Table 8. Results on the parameters of the power law. Fits to the FIRAS data with the revised calibration, errors at 95% CL (parabolic approximation errors for $\log k$ and α). We jointly fit T_0 and the two parameters, $\log k$ and α , of the astrophysical monopole approximated with a power law.

Data set	$\Delta T_0(\text{K})/10^{-4}$	$\log k_d$	β	$T_d(\text{K})$	χ^2/DOF
R-FIRAS	-25.45 ± 12.89	-18.67 ± 0.44	0.91 ± 0.15	2.77 ± 0.10	1.187

Table 9. Results on the parameters of the dust emission law. Fits to the FIRAS data with the revised calibration, errors at 95% CL (parabolic approximation error for ΔT_0 and β). We jointly fit T_0 and the three parameters, $\log k_d$, β and T_d , of the astrophysical monopole approximated with a dust emission law.

Data set	$\Delta T_0(\text{K})/10^{-4}$	$\log k$	α	χ^2/DOF
R-FIRAS + I_{F96}	-1.63 ± 0.50	-20.23 ± 0.48	2.19 ± 0.39	2.000

Table 10. Results on the parameters of the power law. Fits to the FIRAS data with the revised calibration and by readding the astrophysical monopole, I_{F96} , quoted by Fixsen et al. 1996, errors at 95% CL. We jointly fit T_0 and the two parameters, $\log k$ and α , of the astrophysical monopole approximated with a power law.

As briefly mentioned in section 2.3, the analysis presented in sections 4, 5 and 6 is minimally affected by the detailed subtraction of the astrophysical monopole in the case of an emissivity function very close to unit at each frequency; this is because, after the subtraction of the unperturbed Planckian CMB spectrum, the astrophysical monopole dominates residual brightness at sub-millimetric wavelengths whereas the contribution of the CMB spectral distortions dominates at millimetric wavelengths.

Clearly, the calibrator emissivity function considered here calls for a relevant millimetric astrophysical foreground or much larger CMB spectral distortions, that are then relevant also at sub-millimetric wavelengths. We then readd the monopole, I_{F96} , derived by Fixsen et al. 1996 to the data described in section 7.1 and try to fit the data so obtained with a combination of a single astrophysical component plus a possibly distorted CMB spectrum.

We start with a single power law plus a pure CMB Planckian spectrum. The results are reported in Table 10: the χ^2/DOF is clearly high.

We try also a fit in terms of a pure blackbody plus of a dust emission law; it gives a very high temperature $T_d \gtrsim 10^2$ K (i.e. $h\nu/kT_d \ll 1$) and $\beta = 0.23 \pm 0.39$ with $\chi^2/\text{DOF} \simeq 2.047$, or, in other words, reduces to the case of a blackbody plus a power law with $\alpha \simeq \beta + 2$ shown in Table 10, (our best fit properly gives $T_d \sim 340$ K and $\log k_d \sim -22.6$ with quite large errors, because the degeneracy between these two parameters in the limit $h\nu/kT_d \ll 1$, and $\Delta T_0(\text{K})/10^{-4} = -1.62 \pm 0.45$, in good agreement with the results of Table 10). In this subsection we will consider then fits with a single power law and CMB distorted spectra.

The results are reported in Tables 11, 12 and 13 respectively in the case of an early and a late heating process and of a combination of them. Again the data are better explained in terms of an early energy injection. On the other hand, for a single dissipation process the χ^2/DOF remains larger than 1.1 and only with a proper combination of an early energy injection and a late cooling process it reduces to a value of about 1.05.

We will discuss in section 7.6 these results from a physical point of view.

7.5 Joint analysis of CMB spectral distortions and millimetric foreground

In the previous subsection we have shown that, even allowing for a combination of two dissipation processes in the thermal history of the universe, the recalibrated FIRAS data can not be fully explained (i.e. the χ^2/DOF remains significantly higher than unit) when we describe the astrophysical monopole in terms of a single component particularly important at sub-millimetric wavelengths. In addition, the results of section 7.3 suggest that a modified blackbody spectrum at a temperature only just above that of the CMB can play a crucial role in the explanation of the recalibrated FIRAS data.

In Table 14 we report then the results of a fit to the recalibrated FIRAS data added to the monopole derived by Fixsen et al. 1996 in terms of a pure CMB Planckian spectrum plus an astrophysical foreground sum of a power law plus a dust emission law approximated by a modified blackbody. As evident, without resorting to any kind of CMB spectral distortions, the addition of a modified blackbody component significantly improves the fit in a way comparable to that obtained by

Data set	$(\Delta\epsilon/\epsilon_i)/10^{-5}$	$\Delta T_0(\text{K})/10^{-4}$	$\log k$	α	χ^2/DOF
heating at $y_h = 5$					
R-FIRAS + I_{F96}	21.98 ± 6.75	-1.15 ± 0.33	-21.36 ± 0.62	3.09 ± 0.50	1.109

Table 11. Results of the fit for the energy injected at $y_h = 5$ by neglecting late dissipations and free-free distortions and for the astrophysical monopole. Fits to the different data sets with the revised calibration and by readding the astrophysical monopole, I_{F96} , quoted by Fixsen et al. 1996, errors at 95% CL. We jointly fit four parameters, T_0 , the $(\Delta\epsilon/\epsilon_i)$ value referring to the early process [$\hat{\Omega}_b = 0.05$] and the two parameters $\log k$ and α of the astrophysical monopole approximated with a power law.

Data set	$(\Delta\epsilon/\epsilon_i)/10^{-5}$	$\Delta T_0(\text{K})/10^{-4}$	$\log k$	α	χ^2/DOF
heating at $y_h \ll 1$					
R-FIRAS + I_{F96}	11.94 ± 4.74	-0.14 ± 0.35	-22.10 ± 0.99	3.66 ± 0.78	1.604

Table 12. Results on the energy injected at $y_h \ll 1$ by assuming no early dissipations and a null free-free distortion parameter y_B and for the astrophysical monopole. Fits to the different data sets with the revised calibration and by readding the astrophysical monopole, I_{F96} , quoted by Fixsen et al. 1996, errors at 95% CL. We jointly fit four parameters, T_0 , the $(\Delta\epsilon/\epsilon_i)$ value referring to the late process and the two parameters $\log k$ and α of the astrophysical monopole approximated with a power law.

including CMB spectral distortions (the fit quality is intermediate between the case of a single early process and the case of a proper combination of an early and a late process in the case of an astrophysical monopole described by a simple power law).

Note that, as found in the fit reported in Table 9, by adding a modified blackbody component, the CMB thermodynamic temperature T_0 recovered by the fit is lower than 2.725 K, being $2.725 \text{ K} - T_0 \sim \text{some mK}$. The microwave absolute temperature will be then lower at wavelengths of some millimeters than at millimetric wavelengths, where this modified blackbody component shows a peak in terms of νI_ν (see also Fig. 8), whereas at sub-millimetric wavelengths the power law component starts to dominate the residual brightness after the subtraction of the Planckian spectrum at the temperature T_0 . Therefore, from a qualitative point of view, a modified blackbody component leaves an imprint in the microwave spectrum similar to that introduced by an early distortion, the kind of CMB distortion that better describes the recalibrated FIRAS data.

Therefore, we think meaningless to fit the data jointly in terms of an additional modified blackbody component and CMB distortions, because there is an ‘‘approximate’’ degeneration between the contributions of these two components to the global monopole. Analogously to the approach of section 4, except for the difference in the assumed astrophysical foreground, we

Data set	$(\Delta\epsilon/\epsilon_i)/10^{-5}$	$\Delta T_0(\text{K})/10^{-4}$	$\log k$	α	χ^2/DOF	
heating at $y_h = 5$ heating at $y_h \ll 1$						
R-FIRAS + I_{F96}	33.43 ± 14.54	-11.31 ± 12.79	-2.41 ± 0.53	-20.34 ± 1.26	2.30 ± 0.98	1.045

Table 13. Results on the energy injected at $y_h = 5$ and at $y_h \ll 1$ by assuming a null free-free distortion parameter y_B and for the astrophysical monopole. Fits to the different data sets with the revised calibration and by readding the astrophysical monopole, I_{F96} , quoted by Fixsen et al. 1996, errors at 95% CL. We jointly fit five parameters, T_0 , the two $(\Delta\epsilon/\epsilon_i)$ values referring to the early and the late process [$\hat{\Omega}_b = 0.05$] and the two parameters $\log k$ and α of the astrophysical monopole approximated with a power law.

Data set	$\Delta T_0(\text{K})/10^{-4}$	$\log k$	α	$\log k_d$	β	$T_d(\text{K})$	χ^2/DOF
R-FIRAS + I_{F96}	-40.06 ± 1.45	-20.56 ± 2.93	2.23 ± 2.25	-18.41 ± 0.04	0.79 ± 0.11	2.84 ± 0.13	1.081

Table 14. Fits to the FIRAS data with the revised calibration and by readding the astrophysical monopole, I_{F96} , quoted by Fixsen et al. 1996 (parabolic approximation errors at 95% CL). We jointly fit six parameters: T_0 , and the five parameters of the astrophysical monopole approximated with a power law plus a dust emission law.

Data set	$(\Delta\epsilon/\epsilon_i)/10^{-5}$	
	heating at $y_h = 5$	heating at $y_h \ll 1$
R-FIRAS + I_{F96}	0.15 ± 5.35	0.006 ± 2.32
$\Delta T_0(\text{K})/10^{-4}$	-40.10 ± 0.16	-40.10 ± 0.17
χ^2/DOF	0.98514	0.98521
<hr/>		
Table 1 (1985-2000) + [R-FIRAS + I_{F96}]	0.52 ± 5.34	0.009 ± 2.32
$\Delta T_0(\text{K})/10^{-4}$	-40.10 ± 0.16	-40.10 ± 0.17
χ^2/DOF	1.09176	1.09238

Table 15. Results on the energy injected at $y_h = 5$ and $y_h \ll 1$ when these two dissipation processes are separately considered. Fits to the different data sets, errors at 95% CL. We jointly fit two parameters: T_0 and the values of $(\Delta\epsilon/\epsilon_i)$ referring to the early or the late process [$\widehat{\Omega}_b = 0.05$].

derive instead the constraints on CMB spectral distortions by keeping the astrophysical monopole fixed to the description represented by the fit results of Table 14.

In Table 15 we report our results in the case of a single (early, at $y_h \simeq 5$, or late, at $y_h \ll 1$) energy dissipation in the thermal history of the universe, by considering only the frequency range of FIRAS and by adding also the recent long wavelength measures of Table 1. In Fig. 6 we show also the constraints set on a single dissipation process occurring at arbitrary epochs in the thermal history of the universe by the recalibrated FIRAS data and compare them with the results based on the calibration with a constant emissivity function (i.e. the data set 1)). As evident, when the astrophysical monopole is “properly” subtracted, the constraints on the fractional energy exchanges are very similar in the two cases. The constraints on $(\Delta\epsilon/\epsilon_i)$ at very high redshifts are also reported in Fig. 3 for a direct comparison with the results based on the data set 1) and 2).

In Table 16 we report our results for the case of the joint analysis of early ($y_h \simeq 5$) and late ($y_h \ll 1$) dissipations, by considering only the frequency range of FIRAS and by taking also into account the recent long wavelength measures of Table 1. In Fig. 7 we show also the constraints set on the energy exchanged at a given (early or late) epoch by allowing for another dissipation process at a different (late or early) epoch when the recalibrated FIRAS data are combined with the recent long wavelength measures. Again, the comparison with the results based on the calibration with a constant emissivity function (i.e. the data set 2), see Fig. 3) does not show particular differences in the constraints on $(\Delta\epsilon/\epsilon_i)$.

Finally, in the case of the FIRAS data calibrated with this non constant emissivity function we find a small reduction of the χ^2/DOF with respect to the case of a constant emissivity function, when FIRAS data are considered alone ($\simeq 0.985$ instead of $\simeq 1$) as well as in combination with long wavelength measures ($\simeq 1.11$ instead of $\simeq 1.13$).

Data set	$(\Delta\epsilon/\epsilon_i)/10^{-5}$		$\Delta T_0(\text{K})/10^{-4}$	χ^2/DOF
	heating at $y_h = 5$	heating at $y_h \ll 1$		
R-FIRAS + I_{F96}	0.44 ± 9.72	-0.15 ± 4.21	-40.11 ± 0.30	1.007
Table 1 (1985-2000) + [R-FIRAS + I_{F96}]	1.65 ± 9.67	-0.59 ± 4.19	-40.14 ± 0.29	1.108

Table 16. Results on the energy injected at $y_h = 5$ and $y_h \ll 1$ when these two dissipation processes are jointly considered. Fits to the different data sets, errors at 95% CL. We jointly fit three parameters: T_0 and the two values of $(\Delta\epsilon/\epsilon_i)$ referring to the early and late process [$\widehat{\Omega}_b = 0.05$].

7.6 Cosmological and astrophysical implications

The explanation of the FIRAS data recalibrated according to Battistelli et al. (2000) in terms of pure CMB spectral distortions seems to be difficult. From the point of view of the data analysis, the better solution in this scheme involves a small modification of the astrophysical monopole with respect to that given by Fixsen et al. 1996, I_{F96} , (clearly compatible with the current models for the sub-millimetric extragalactic foreground generated by distant galaxies) and a relevant early energy injection, $\Delta\epsilon/\epsilon \sim 3 \times 10^{-4}$, which effect on the spectrum has to be partially modified by a late cooling process associated to an energy exchange smaller by a factor ~ 3 , $\Delta\epsilon/\epsilon \sim 10^{-4}$, to give a χ^2/DOF quite close to unit (see Tables 11 and 13). We have also tested that an energy injection at intermediate values of y_h does not improve but worsens the fit quality with respect to the results of Tables 11 and 13. A vacuum decay with a radiative channel can not explain this result because it predicts a late positive energy dissipation much larger than the early one (see, e.g., Freese et al. 1987, Weinberg 1988, Bartlett & Silk 1989, Overduin et al. 1993). The damping of adiabatic perturbations (Sunyaev & Zeldovich 1970) may generate a relevant early distortion (Daly 1991, Barrow & Coles 1991, Burigana 1993, Hu et al. 1994), but, unfortunately, only for cosmological parameters excluded by the recent CMB anisotropy experiments (see, e.g., Netterfield et al. 2002, Stompor et al. 2001, Pryke et al. 2002, and references therein). Also the damping of isocurvature perturbations seems to be not able to generate such kind of distortion, because the high density contrast predicted at high redshifts is expected to significantly increase the Bremsstrahlung efficiency in erasing early distortions, so that the generation of a late distortion larger than the early one is favourite (Daly 1991, Burigana 1993). Radiative decays of massive particles (Silk & Stebbins 1983) at early times, with appropriate number density, mass, lifetime and branching ratio may produce such kind of early distortion. On the other hand, a proper balance between the parameters of the early decay and of a completely different cooling process at late epochs or a delicate fine tuning of the decay parameters at intermediate epochs, able to accurately reproduce the required spectral shape (see, e.g., Danese & Burigana 1993) without affecting the evolution of the red giant branch (Raffelt et al. 1989), is required for a full explanation of the data, otherwise the χ^2/DOF is larger than unit of about the 10%. Of course these possibilities can not be excluded, but they seem quite unrealistic or, at least, quite weak.

Measurements at $\lambda \approx 5.64\widehat{\Omega}_b^{-2/3}$ cm may in principle play a relevant role for the understanding of early distortions, being there maximum the amplitude of the BE-like distortions, $(\Delta T/T)_m \simeq 5.82\mu(y_h \simeq 5)\widehat{\Omega}_b^{-2/3}$ (Burigana et al. 1991a). Unfortunately, the error bars \dagger of the current measures at $\lambda \gtrsim 20$ cm are much larger (by about one order of magnitude, see Table 1) than the maximum distortion of about 50–100 mK compatible with the upper limit (at 95% CL) on $\mu(y_h \simeq 5)$ ($\simeq 1.4\Delta\epsilon/\epsilon_i$) derived here in the case of the calibration of FIRAS data by Battistelli et al. (2000) for $\widehat{\Omega}_b$ compatible with recent CMB anisotropy experiments and the big-bang nucleosynthesis. A great improvement of long wavelength spectrum measurements is therefore necessary for consistency tests of FIRAS calibration.

If we allow for a further component to the astrophysical foreground, relevant at millimetric wavelengths, quite well approximated by a dust emission law with modified blackbody parameters close to those of Table 14 (to be considered only as a simple set of observational/phenomenological parameters), the recalibrated FIRAS data can be properly explained by including CMB spectral distortions generated by dissipation processes with energy exchanges ($\Delta\epsilon/\epsilon \approx 10^{-5}$, compatible with null values) consistent with current cosmological scenarios, both at early and late epochs, without requiring a proper balance

\dagger According to the considered frequency and observational method, the major contributions to the experimental uncertainty of long wavelength spectrum measurements derive from instrumental effects and/or atmospheric and foreground contamination (see, e.g., Sironi et al. 1990, 1991, Bensadoun et al. 1993, Bersanelli et al. 1994, Salvaterra & Burigana 2000, and references therein).

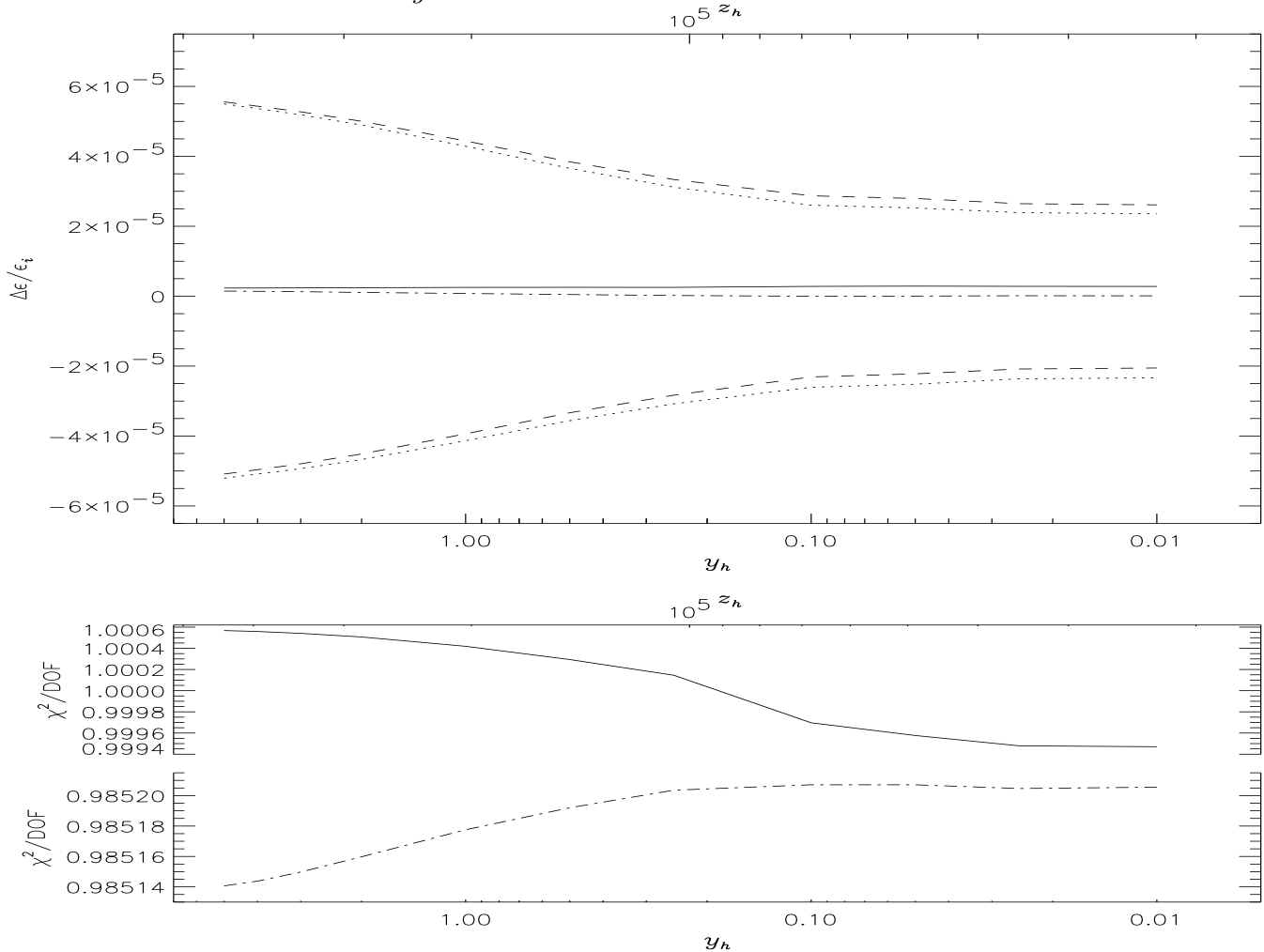


Figure 6. The same as in Fig. 1, but with reference to the exploitation of the data set 1) (solid lines and dashed lines) and of the FIRAS data alone but calibrated according to Battistelli et al. (2000) by adding the “experimental” astrophysical monopole, I_{F96} , derived by Fixsen et al. (1996) and subtracting the “theoretical” astrophysical monopole of the best fit obtained assuming a power law plus a dust emission law as in Table 14 (dot-dashed lines and dotted lines) [$\widehat{\Omega}_b = 0.05$].

between the energy possibly injected at different cosmic times to obtain a χ^2/DOF extremely close to unit. We consider then the astrophysical implications of this scheme.

In Fig. 8 we compare the brightness of the dust emission component, $I_{D_{bf}}$, represented by the best fit reported in Table 14 with the sub-millimetric foreground as derived by Fixsen et al. 1996 and by Fixsen et al. 1998, the predictions based on the models by Toffolatti et al. 1998 and by Guiderdoni et al. 1998, the brightness of the Galaxy at Pole as found by Fixsen et al. 1996 (extended in the figure up to sub-millimetric frequencies) and the power law component represented by the best fit reported in Table 14.

The comparison of the brightness integrated over the frequencies of the dust emission component $I_{D_{bf}}$ with the CMB integrated brightness gives $\int I_{D_{bf}} d\nu / \int B_\nu(T_0) d\nu \sim 1/170 \sim 4\Delta T_0/T_0$ (where $\Delta T_0 \simeq 4\text{mK}$, see Table 14); this value, much larger than the upper limits on $\Delta\epsilon/\epsilon_i$ reported in Tables 5–7 and 11–13, is simply due to the lower best fit value of T_0 found in this case. Analogously, the brightness integrated over the frequencies of the dust emission component $I_{D_{bf}}$ is about 1/4 of the integrated brightness of the Galaxy at Pole component found by Fixsen et al. 1996 (extrapolated up to sub-millimetric wavelengths), $\int I_{D_{bf}} d\nu / \int I_{GP} d\nu \sim 1/4$. By comparing $I_{D_{bf}}$ with the the extragalactic sub-millimetric foreground generated by the distant galaxies, as derived by Fixsen et al. 1998, we find $\int I_{D_{bf}} d\nu / \int I_{F98} d\nu \sim 1/3$. So, there are no particular problems from the energetic point of view for an explanation of this millimetric component in terms of emission from cold dust in an extended halo around our Galaxy or around distant galaxies; in the latter case the high isotropy level of this component at angular scales larger than few degrees is simply explained. Unfortunately, a direct detection of millimetric emission quite far from the central regions of distant dusty galaxies seems very difficult with current millimetric telescopes.

Assuming that a fraction f of the cold dust producing this millimetric foreground is located around distant dusty galaxies, an approximate estimate of the corresponding Poisson rms fluctuation level, $\sigma_{D_{bf}}$, can be simply derived by rescaling the

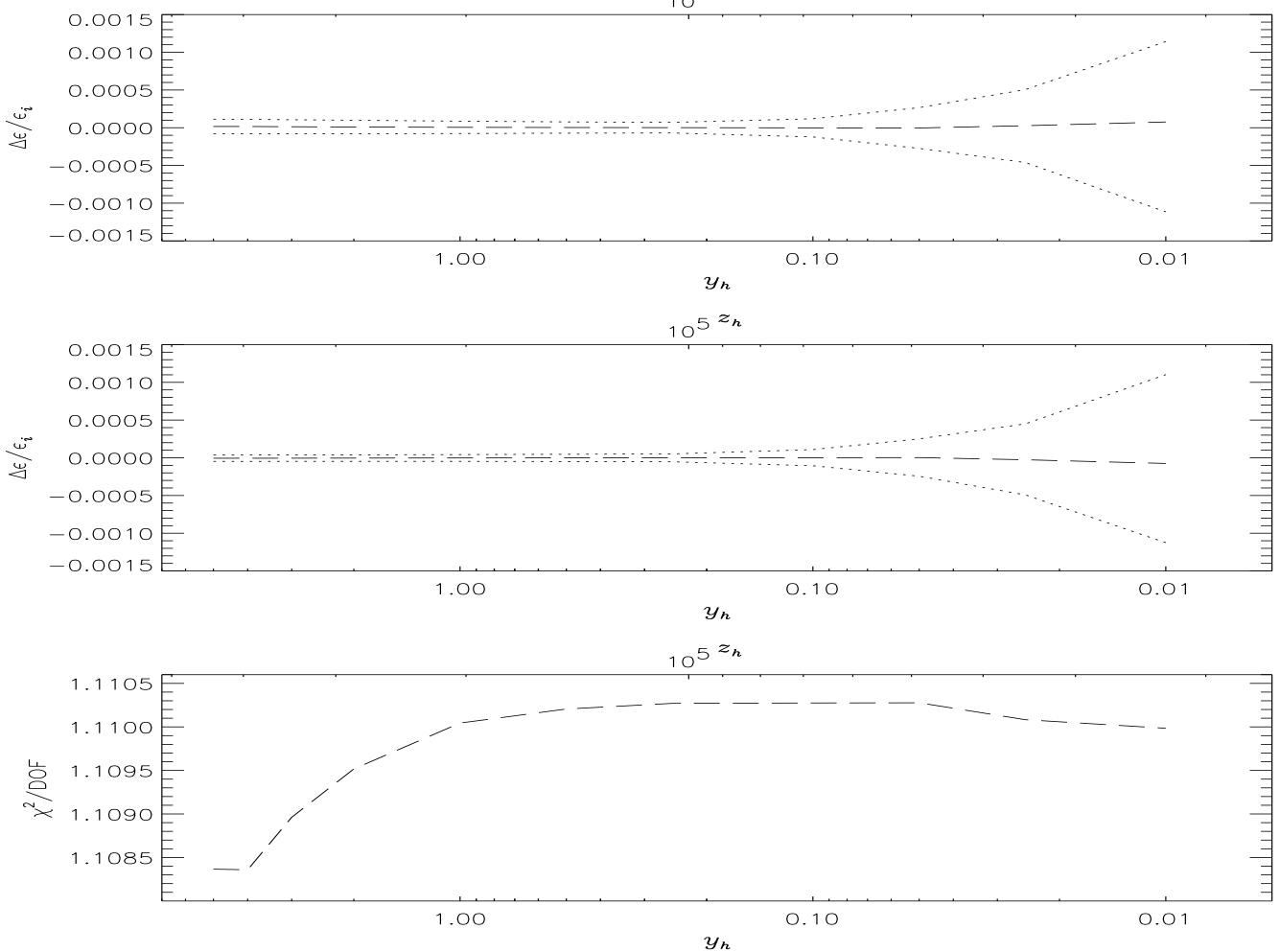


Figure 7. The same as in Fig. 3, but with reference to the exploitation of the FIRAS data alone but calibrated according to Battistelli et al. (2000) by adding the “experimental” astrophysical monopole, I_{F96} , derived by Fixsen et al. (1996) and subtracting the “theoretical” astrophysical monopole of the best fit obtained assuming a power law plus a dust emission law (see Table 14) jointed to the recent ground and balloon measures [$\widehat{\Omega}_b = 0.05$].

usual rms fluctuation, σ_{dg} , of dusty galaxies. For differential number counts approximately described by a power-law form, $dN(S)/dS \simeq gS^{-(\gamma+1)}$, the rms fluctuation is given by $\simeq q^{(2-\gamma)/\gamma} (g\omega_e)^{1/\gamma} / (2-\gamma)^{1/\gamma}$, where ω_e is the antenna beam pattern effective solid angle and sources above the chosen $q - \sigma$ clipping detection limit (being σ the rms confusion noise from all contributions and $q \sim 2.5 \div 5$) are removed (De Zotti et al. 1996). The ratio between the level of the contribution to this millimetric foreground associated to halos around distant dusty galaxies and the sub-millimetric foreground extrapolated at millimetric wavelengths is given by rf , where r ranges from ~ 20 to 100 for ν from ~ 300 to 100 GHz (see Fig. 8). Assuming the same typical ratios, rf , for the corresponding source intrinsic components, we have that the value of g relevant for the millimetric number counts, g_{Dbf} , is related to that relevant for the sub-millimetric number counts, g_{dg} , by $g_{Dbf} \sim (rf)^{(\gamma+1)} g_{dg}$, and then $\sigma_{Dbf} \sim (rf)^{(\gamma+1)/\gamma} \sigma_{dg}$. Assuming $\gamma = 1.25 \div 1.5$ and the current estimates of the combined rms fluctuation from dusty galaxies and radiogalaxies, σ_{ex} , at these frequencies (Toffolatti et al. 1999), we find $\sigma_{Dbf} \sim (20 \div 15) \sigma_{ex}$ (or $\sigma_{Dbf} \sim (4.5 \div 3) \sigma_{ex}$) even for $f \sim 0.25$ (or ~ 0.1). A significant excess in the angular power spectrum at high multipoles is then unavoidable in this scheme, unless galactic outflows and/or interactions efficiently redistribute the cold dust more uniformly in the intergalactic medium. It should be observable with the current space anisotropy experiment MAP[§] by NASA, and, with a wide frequency coverage, with the PLANCK satellite[¶] by ESA even for quite small values of f ($f \sim 0.07$).

On the other hand, the implications for the dust mass involved in this scenario is critical. The value of k_d derived from the fit (see Table 14) is about 1500 times larger than the analogous parameter corresponding to the monopole, I_{F98} , derived by Fixsen et al. 1998. Therefore, the involved mass of cold dust around distant galaxies (or its intrinsic emissivity) should be

[§] <http://map.gsfc.nasa.gov/>

[¶] <http://astro.estec.esa.nl/Planck>

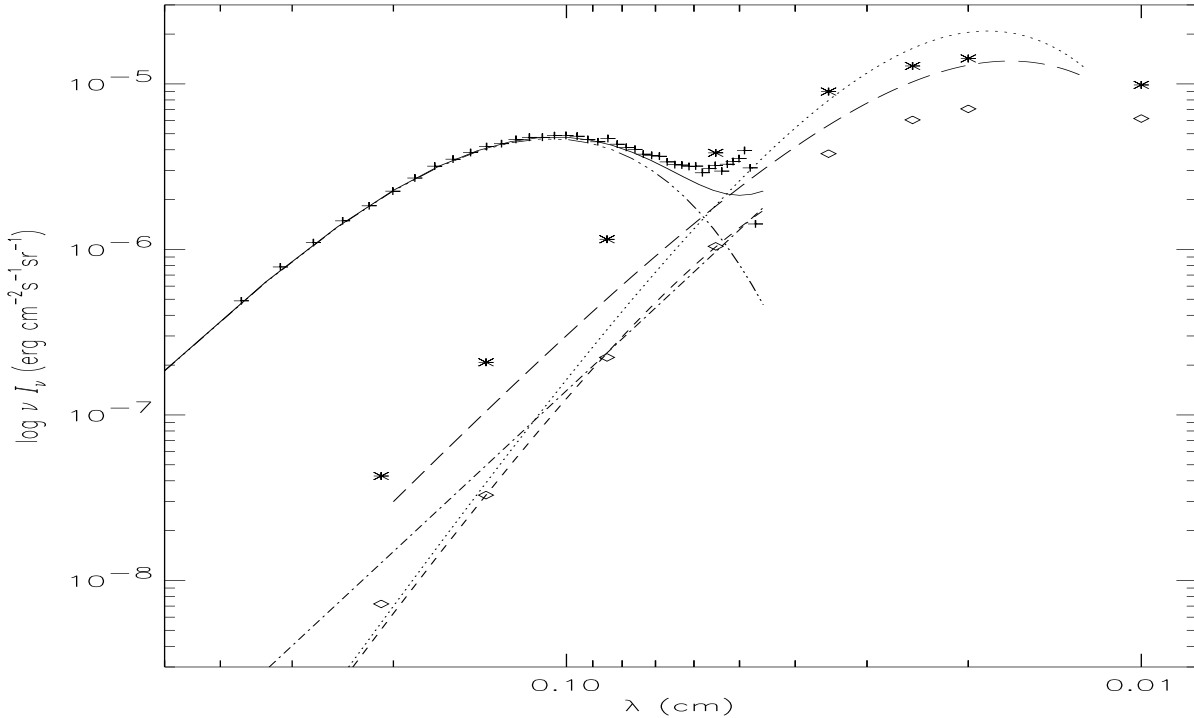


Figure 8. Comparison between the brightness of the dust emission component, I_{Dbf} , of the best fit reported in Table 14 (three dots/dash) and the sub-millimetric foreground as derived by Fixsen et al. 1996 (dashed line) and by Fixsen et al. 1998 (long dashes), the predictions based on the models of Toffolatti et al. 1998 (diamonds) and of Guiderdoni et al. 1998 (asterisks), the brightness of the Galaxy at Pole as found by Fixsen et al. 1996 (extended in the figure up to sub-millimetric frequencies, dotted line) and with the power law component, I_{PLbf} , represented by the best fit reported in Table 14 (dot-dashed line). We report also the sum of I_{Dbf} and I_{PLbf} (solid line) compared to the LLSS FIRAS data of Fixsen et al. 1996, including the monopole I_{F96} , but calibrated according to Battistelli et al. 2000 after the subtraction of a blackbody at the best fit temperature $T_0 \simeq 2.721$ reported in Table 14 (crosses). The 1σ uncertainty of these data is not reported being less than $\sim 10^{-7}$ erg cm $^{-2}$ sec $^{-1}$ sr $^{-1}$ at the wavelengths $\lambda \gtrsim 700\mu\text{m}$ relevant for the evaluation of the considered millimetric foreground. As evident, the shape and level of I_{Dbf} at $\lambda \gtrsim 700\mu\text{m}$ does not critically depend on the details of the subtraction of the sub-millimetric contribution from distant galaxies.

orders of magnitude larger than that producing the sub-millimetric foreground. Of course, an analogous mass problem holds for a cold dust halo around the Galaxy. This problem can be overcome by considering cold dust at low redshifts ($z \approx 0.1$), but in this case the anisotropy problem described above seems even more critical, since an efficient dust redistribution at low redshifts is unrealistic; in addition, we should find observational evidences at low redshifts.

8 CONCLUSIONS

In this work we have compared the absolute temperature data of the CMB spectrum with models for CMB spectra distorted by a single or two heating processes at different cosmic times.

We have computed the limits on the amount of the energy injected in the radiation field for the whole range of cosmic epochs, expressed here in terms of the dimensionless time variable y_h . These upper and lower limits on $\Delta\epsilon/\epsilon_i$ are mainly provided by the precise measures of the FIRAS instrument aboard the COBE satellite. The addition of the data obtained from ground and balloon experiments at longer wavelengths does not alter significantly the results based on the FIRAS data alone, because of the large error bars of the measures at $\lambda \gtrsim 1$ cm. We analyzed also the impact of the FIRAS calibration on the determination of $\Delta\epsilon/\epsilon_i$ when the FIRAS data are used together with the ground and balloon measures: the uncertainty of 2 mK at 95% CL in the FIRAS calibration (Mather et al. 1999) does not affect significantly the limits on $\Delta\epsilon/\epsilon_i$. From the χ^2 analysis, the lower limit at 2.723 K results weakly favourite. This is due to the well known disagreement between the absolute temperature of the FIRAS data and of the mean temperature of the data at $\lambda > 1$ cm.

We considered different values of the baryon density. For the same y_h , the value of Ω_b does not significantly influence the upper and lower limits on the amount of the injected energy (of course, $z_h(y_h)$ decreases with Ω_b).

As in the case of a single heating, we exploit the CMB spectrum data under the hypothesis of two heating processes

occurred at different epochs, the former at any y_h in the range $5 \geq y_h \geq 0.01$ (but only for $y_h \gtrsim 0.1$ this analysis results to be meaningful) and the latter at $y_h \ll 1$. The limits on $\Delta\epsilon/\epsilon_i$ are relaxed by a factor ~ 2 both for the earlier and the later process with respect to the case in which a single energy injection in the thermal history of the universe is considered.

Also in this case, we analyzed the impact of the FIRAS calibration and the role of the baryon density. The results are very similar to those obtained for the case of single heating.

In general, the constraints on $\Delta\epsilon/\epsilon_i$ are weaker for early processes ($5 \gtrsim y_h \gtrsim 1$) than for relatively late processes ($y_h \lesssim 0.1$), because of the sub-centimetric wavelength coverage of FIRAS data, relatively more sensitive to Comptonization than to Bose-Einstein like distortions.

We evaluate also the limits on $\Delta\epsilon/\epsilon_i$ for energy injections occurring during the kinetic equilibrium period (i.e. at $z \gtrsim z_1$). By allowing for a further late dissipation process, the constraints on $\Delta\epsilon/\epsilon_i$ at $z \gtrsim z_1$ return to be relaxed with respect to the case of a single injection at high z , particularly at $z_1 \lesssim z \lesssim z_{therm}/2$ (up to a factor ~ 2).

In conclusion, the available data permit to set very stringent constraints on the energy injected in the radiation field at different cosmic times, mainly set by the precise measures of FIRAS.

On the other hand, measures at $\lambda \gtrsim 1$ cm, where significant improvements are needed, play a crucial role to probe free-free distortions and to better constrain the thermal history of the universe at late epochs.

We carefully considered also the implications of the FIRAS calibration as revised by Battistelli et al. 2000. From a widely conservative point of view (i.e. allowing for the whole set of calibrator emissivity curves reported by the authors), it only implies a significant relaxation of the constraints on the Planckian shape of the CMB spectrum. On the other hand, the favourite calibrator emissivity law proposed by the authors, when used to recalibrate the FIRAS data, implies significant deviations from a Planckian spectrum. If interpreted in terms of CMB spectral distortions, the full data set can be explained only by assuming a proper balance between the energy exchanges at two completely different cosmic times or a delicate fine tuning of the parameters of a dissipation process at intermediate epochs, possibly in form radiative decays of massive particles. The interpretation in terms of a relevant millimetric foreground, quite well described by a modified blackbody law as in the case of emission from cold dust, does not present this problem, the constraints on energy exchanges in the primeval plasma being close to those derived above by assuming a constant emissivity of the calibrator. On the other hand, the too large mass of dust required in this scenario and/or the significant increase of the fluctuations at sub-degree angular scales represent again a very difficult problem. While a careful control of the calibration of CMB spectrum observations at this high level of sensitivity is essential to establish limits on (or measure) $\Delta\epsilon/\epsilon_i$ with an accuracy of $\sim 10^{-5} \div 10^{-4}$, our analysis indicates that it is very difficult to explain a non constant FIRAS calibrator emissivity law with a spectral dependence close to that considered here.

Future precise measurements at longer wavelengths, particularly significant for early dissipation processes, as well as current and future CMB anisotropy space missions will provide independent, direct or indirect, cross checks.

ACKNOWLEDGEMENTS

It is a pleasure to thank M. Bersanelli, D.J. Fixsen, N. Mandolesi, C. Macculli and G. Palumbo for useful discussions on CMB spectrum observations. We warmly thank L. Danese, G. De Zotti and L. Toffolatti for constructive and stimulating comments and the fruitful long-term collaboration on CMB spectral distortions and astrophysical foregrounds. We wish to thank the referee for valuable comments.

REFERENCES

Bartlett J.G. & Silk J. 1989, Proceedings of the "Workshop on Particle Astrophysics: Forefront Experimental Issues", ed. E.B. Norman, World Scientific, Singapore, pg. 132

Battistelli E.S., Fulcolli V., Macculli C. 2000, New Astronomy, 5, 77

Bensadoun M., Bersanelli M., de Amici G. et al. 1993, ApJ, 409, 1

Bersanelli M., Witebsky C., Bensadoun M. et al. 1989, ApJ, 339, 632

Bersanelli M., Bensadoun M., de Amici G. et al. 1994, ApJ, 424, 517

Boynton P.E., Stokes R.A., Wilkinson D.T. 1968, Phys. Rev. Lett., 21, 462

Boynton P.E. & Stokes R.A. 1974, Nature, 247, 528

Burigana C. 1993, PhD thesis, Univ. Padova

Burigana C., Danese L., De Zotti G. 1991a, A&A, 246, 59

Burigana C., De Zotti G., Danese L. 1991b, ApJ, 379, 1

Burigana C., De Zotti G., Danese L. 1995, A&A, 303, 323

Burigana C., Danese L., De Zotti G. et al. 1997, MNRAS, 287, L17

Burigana C. & Popa L. 1998, A&A, 334, 420

Burigana C. & Salvaterra R. 2000, Int. Rep. ITeSRE/CNR 291/2000, August

COBE/FIRAS Explanatory Supplement, eds. Mather J.C. et al. 1995, COBE Ref. Pub. No.95-C

Daly R.A. 1991, *ApJ*, 371, 14

Danese L. & Burigana C. 1993, in: "Present and Future of the Cosmic Microwave Background", Lecture in Physics, Vol. 429, eds. J.L. Sanz, E. Martinez-Gonzales, L. Cayon, Springer Verlag, Heidelberg (FRG), p. 28

Danese L. & De Zotti G. 1977, *Riv. Nuovo Cimento*, 7, 277

De Amici G., Smoot G.F., Friedman S.D., Witebsky C., 1985, *ApJ*, 298, 710

De Amici G., Limon M., Smoot G.F. et al. 1991, *ApJ*, 381, 341

De Zotti G., Toffolatti L., Argüeso Gómez F. et al., 1999, Proceedings of the EC-TMR Conference "3 K Cosmology", Roma, Italy, 5-10 October 1998, AIP Conference Proc. 476, Maiani L., Melchiorri F., Vittorio N., (Eds.), pg. 204, astro-ph/9902103

De Zotti G., Franceschini A., Toffolatti L., Mazzei P., Danese L. 1996, *Astroph. Lett. and Comm.*, 35, 289

Ewing M.S., Burke B.F., Staelin D.M. 1967, *Phys. Rev. Lett.*, 19, 1251

Fixsen D.J., Cheng E.S., Cottingham D.A. et al. 1994, *ApJ*, 420, 457

Fixsen D.J., Cheng E.S., Gales J.M. et al. 1996, *ApJ*, 473, 576

Fixsen D.J., Dwek E., Mather J.C., Bennett C.L., Shafer R.A. 1998, *ApJ*, 508, 123

Franceschini A., Mazzei P., De Zotti G., Danese L. 1994, *ApJ*, 427, 140

Freese K., Adams F.C., Frieman J.A., Mottola E. 1987, *Nucl. Phys. B*287, 797

Guiderdoni B., Hivon E., Bouchet F.R., Maffei B. 1998, *MNRAS*, 295, 877

Howell T.F. & Shakeshaft J.R. 1966, *Nature*, 210, 1318

Howell T.F. & Shakeshaft J.R. 1967, *Nature*, 216, 753

Hu W., Scott D., Silk J. 1994, *ApJ*, 430, L5

Johnson D.G. & Wilkinson D.T. 1987, *ApJ*, 313, L1

Kislyakov A.G., Chernyshev V.I., Lebskii Yu.V., Mal'tsev V.A., Serov N.V. 1971, *Sov. Ast.*, 15, 29

Kogut A., Witebsky C., Bensadoun M. et al. 1988, *ApJ*, 325, 1

Kogut A., Bensadoun M., de Amici G. et al. 1990, *ApJ*, 355, 102

Kompaneets A.S. 1956, *Zh. Eksp. Teor. Fiz.*, 31, 876 [Sov. Phys. JEPT, 4, 730, (1957)]

Levin S.M., Witebsky C., Bensadoun M. et al. 1988, *ApJ*, 334, 14

Levin S.M., Bensadoun M., Bersanelli M. et al. 1992, *ApJ*, 396, 3

Mandolesi N., Calzolari P., Cortiglioni S. et al. 1986, *ApJ*, 310, 561

Mather J.C., Cheng E.S., Eplee R.E.Jr. et al. 1990, *ApJ*, 354, L37

Mather J.C., Cheng E.S., Cottingham D.A. et al. 1994, *ApJ*, 420, 439

Mather J.C., Fixsen D.J., Shafer R.A., Mosier C., Wilkinson, D.T. 1999, *ApJ*, 512, 511

Mennella V., Brucato J.R., Colangeli L. et al. 1998, *ApJ*, 496, 1058

Millea M.F., McColl M., Pedersen R.J., Vernon F.L. 1971, *Phys. Rev. Lett.*, 26, 919

Netterfield C.B., Ade P.A.R., Bock J.J. et al. 2002, *ApJ*, 571, 604

Nordberg H.P. & Smoot G.F. 1998, astro-ph/9805123

T.Y. Otoshi & C.T. Stelzreid 1975, *IEEE Trans. on Inst. & Meas.*, 24, 174

Overduin J.M., Wesson P.S., Bowyer S. 1993, *ApJ*, 404, 1

Pelyushenko S.A. & Stankovich K.S. 1969, *Sov. Astr.*, 13, 223

Penzias A.A. & Wilson R.W. 1965, *ApJ*, 142, 419

Penzias A.A. & Wilson R.W. 1967, *ApJ*, 72, 315

Pryke C., Halverson N.W., Leitch E.M., et al. 2002, *ApJ*, 568, 46

Platania P., Burigana C., De Zotti G., Lazzaro E., Bersanelli M. 2002, *MNRAS*, submitted, astro-ph/0206079

Puget J.L., Abergel A., Bernard J.P. et al. 1996, *A&A*, 308, 5

Puzanov V.I., Salomonovich A.E., Stankovich K.S. 1968, *Sov. Astr.*, 11, 905

Raffelt G., Dearborn D., Silk J. 1989, *ApJ*, 336, 61

Raghunathan A. & Subrahmanyan R. 2000, *Journ. of Astroph. & Astron.*, 21, 1, astro-ph/0005297

Roll P.G. & Wilkinson D.T. 1966, *Phys. Rev. Lett.*, 16, 405

Sadat R., Guiderdoni B., Silk J. 2001, *A&A*, 369, 26

Salvaterra R. & Burigana C. 2000, *Int. Rep. ITeSRE/CNR* 270/2000, March, astro-ph/0206350

Schuster J.A. 1993, PhD Thesis, UC Berkeley

Silk J. & Stebbins A. 1983, *ApJ*, 269, 1

Sironi G., Limon M., Marcellino G. et al. 1990, *ApJ*, 357, 301

Sironi G., Bonelli G., Limon M. 1991, *ApJ*, 378, 550

Staggs S.T., Jarosik N.C., Wilkinson D.T., Wollack E.J. 1996a, *ApJ*, 458, 407

Staggs S.T., Jarosik N.C., Meyer S.S., Wilkinson D.T. 1996b, *ApJ*, 473, L1

Stankevich K.S., Wielebinski R., Wilson W.E. 1970, *Australian J. Phys.*, 23, 529

Stokes R.A., Partridge R.B., Wilkinson D.T. 1967, *Phys. Rev. Lett.*, 19, 1199

Stompor R., Abroe M., Ade P., et al. 2001, *ApJ*, 561, L7

Sunyaev R.A. & Zeldovich Ya.B. 1970, *Ap&SS*, 7, 20

Toffolatti L., Argüeso Gómez F., De Zotti G. et al. 1998, *MNRAS*, 297, 117

Weinberg S. 1989, *Rev. Mod. Phys.*, Vol. 61, No. 1, 1

Welch W.J., Keachie S., Thornton D.D., Wrixon G. 1967, *Phys. Rev. Lett.*, 18, 1068

Wilkinson D.T. 1967, *Phys. Rev. Lett.*, 19, 1195

Zeldovich Ya.B. & Sunyaev R.A. 1969, *Ap&SS*, 4, 301

Zeldovich Ya.B., Illarionov A.F., Sunyaev R.A. 1972, *Zh. Eksp. Teor. Fiz.*, 62, 1216 [Sov. Phys. JEPT, 35, 643]